Report No. UT-02.18

STRUCTURAL CONDITION ASSESSMENT USING DYNAMIC TESTING I-15 TESTBED RESEARCH, PHASE II

FINAL REPORT

Submitted by:

Department of Civil & Environmental Engineering, Utah State University

Utah Department of Transportation
Research Division

March 2003

UDOT RESEARCH & DEVELOPMENT REPORT ABSTRACT

1. Report No. UT-02.18	2. Govern. Accession No.	3. Recipient's Catalog No.
4. Title and Subtitle STRUCTURAL CONDITION ASSESSMENT USING DYNAMIC TESTING I-15 TESTBED RESEARCH, PHASE II	5. Report Date March, 2003	
	6. Performing Organization Code	
7. Author(s) Halling, Marvin W.; Bay, James A.; Womack, Kevin C.; Achter, Jeremy; Robinson, Marc; Gottipati, Aravind; Huber, Michael; Christensen, Colby.	8. Performing Organization Report No.	
9. Performing Organization Name and Address Department of Civil and Environmental Engineering Utah State University Logan, Utah 84322-4110	10. Work Unit No.	
	11. Contract or Grant No. Contract 00-9111	
12. Sponsoring Agency Name and Address Utah Department of Transportation 4501 South 2700 West Salt Lake City, Utah	13. Type of Report and Period Covered Final Report, July 2000 – December 2002	
	14. Sponsoring Agency Code: 81F15025	
15. Supplementary Notes		
16. Abstract Several bridges were instrumented with accelerometers and were vibrated using harmonic forcing and impact forcing. Modal parameters were determined and monitored during the entire process. Damage was inflicted on the structures and then the structures were re-tested in the damaged states. Changes in the modal parameters were noted and analyzed. The method is designed to detect if damage has occurred, determine the intensity of the damage, and the location of the damage.		
17. Key Words condition assessment, structural health monitoring, strong motion instruments, bridge instrumentation, dynamic modal testing.	18. Distribution Statement	
19. Security Classification (of this report) None	20. Security Classification (of this page) None	21. No. of Pages 57	22. Price

STRUCTURAL CONDITION ASSESSMENT USING DYNAMIC TESTING
I-15 TESTBED RESEARCH PHASE II

A Research Report Submitted to the
Utah Department of Transportation
UT-02.18

By

Marvin W. Halling
James A. Bay
Kevin C. Womack
Jeremy Achter
Marc Robinson
Aravind Gottipati
Michael Huber
Colby Christensen

Department of Civil and Environmental Engineering
Utah State University
Logan, UT

March 2003

Table of Contents

LIST OF FIGURES

List of Tables

CHAPTER 1

Executive Summary and Implementation

This report summarizes the dynamic testing that was conducted at three sites along the I-15 corridor in Salt Lake City from July 2000 to November 2002. The three sites are the bridge bents at 600 South, the six span segment of the 500 South viaduct, and the three span bridge at 300 North.

The chapters have been organized in the following order: Chapter 2 contains the description of the harmonic forced vibration testing on the bents at 600 South, Chapter 3 contains the description of the harmonic forced vibration testing of the viaduct at 500 South, Chapter 4 contains the description of the numerical modeling of the viaduct at 500 South, Chapter 5 is a description of the impact testing of both the bents at 600 South as well as the viaduct at 500 South, and Chapter 6 is a description of the harmonic forced vibration testing of the bridge at 300 North. Each chapter contains its own description of the work done, the analysis, and conclusions.

This work is early work in the development of additional techniques for the evaluation and maintenance of bridge structures. Dynamic techniques also have applications in the determination of existing boundary conditions, bearing function, and overall changes in the stiffness of a bridge.

1.1 OVERVIEW OF THE PROJECT

Dynamic damage detection is intended to be able to determine if damage has occurred in a given structure, and if so, to be able to determine where it has occurred. The method focuses on the dynamic characteristics of the structure, namely, the modal natural frequencies, the mode shapes, and the modal damping. Each of these dynamic characteristics would be expected to change with damage, because of their dependence on the mass, the damping coefficients, and the stiffness of the structure. Of particular interest is the localized change in stiffness in a structure due to damage.

Theoretically, if a structure were known completely, i.e. the mass matrix, the damping matrix, and the stiffness matrix completely determined, then any change in any one of these matrices would lead to identification of damage and the determination of its location.

However, in real civil structures, the complexities make it impossible to create an exact model. There are significant uncertainties in both the real structure and the models of the structure. These uncertainties are the reason for the difficulties in exactly identifying damage in an actual structure.

Dynamic characteristics can be determined experimentally using several types of forced vibration techniques or ambient vibration techniques. As in all experiments, there are sources of error and variability in the tests. The combination of experimental error, and testing variability make it difficult to

determine whether or not small changes in measured response quantities are encompassed within the range of experimental errors and testing variability or whether the changes can be attributed to actual changes in the structure (damage).

The demolition of the "old" I-15 structures provided an excellent opportunity to experimentally determine dynamic characteristics of a healthy structure, and then intentionally inflict a known quantity of damage to the structure. Following the damage, the experimental procedure was repeated. This was conducted on several structures with each structure being submitted to several "states" of damage.

1.2 RESULTS

This work is significant for several reasons.

First: We have shown in the studies that are included in this report that damage inflicted on real civil structures can be detected by tracking the changes in the modal frequencies of the lower modes. These lower modes are typically considered to be the lowest eight to ten modes of the structure.

Second: The studies included in this report investigate the use of several structural forcing techniques. These techniques include harmonic forced vibration using an eccentric-mass shaking machine bolted to the structure, impact load testing utilizing a swinging 450 lb hammer, and impact load testing utilizing a 10 lb hammer. Also successfully used in other studies are an electro-magnetic shaker and ambient vibrations.

Third: These studies have tracked the degradation of actual structures through various states of damage. This has been of great value because of the extremely limited data set available that includes damage states of actual civil structures.

1.3 IMPLEMENTATION

The anticipated implementation of the current research is in the area of continued investment into long term monitoring of the transportation system for the State of Utah. The results described in this report are optimistic that the investment of money into instrumentation and monitoring of the infrastructure will lead to better information regarding the function and health of the system and will facilitate decision making in the future. The future health of the system will be affected by slow moving damage (age deterioration of components), which is encompassed in the overall goals of asset management, as well as faster acting damage such as earthquake, impact, scour, wind, or other damage mechanisms.

The authors strongly recommend that the Utah Department of Transportation support an ongoing program of health monitoring instrumentation including an assortment of sensors. These instruments should include strong motion arrays (accelerometers), geotechnical monitoring devices for settlement, slope stability, bridge pressures, etc., and other structural and pavement embedded and non-embedded devices.

The closely monitored systems in the future will lead to a more “intelligent” management of the transportation for the State.

CHAPTER 2

Bridge Bents at 600 South

Dynamic testing results from full-scale bridges and their components are few according to Salawu and Williams (1995). The recent redesign and reconstruction of the I-15 corridor through Salt Lake City provided an assortment of full-scale test specimens. Currently, Utah State University is conducting research on the use of forced vibration testing along with modal analysis as a non-destructive condition assessment tool. This research addresses the effects of various states of damage on the modal parameters of reinforced concrete bridge bents and the potential for finite element modeling to accurately portray the field results. Of the several structures under investigation at Utah State University, the 600 South viaduct served as the test region for this portion of the research. The 600 South viaduct was an elevated, two-lane roadway that served as the primary access to downtown Salt Lake from I-15. During demolition, three reinforced concrete bridge bents were left standing and intact after the deck had been removed. These bents served as the research specimens.

2.1 INTRODUCTION

In recent history, earthquake engineering has been pushed to the forefront of the structural engineering community. Design codes are constantly being revised and upgraded to make the infrastructure in seismic zones safe. Rather than simply padding the safety factors for design, the professional world and the academic world both want to know what happens when a structure is subjected to strong, damaging earthquake forces. There are currently several techniques in use for determining dynamic characteristics of structures. Forced vibration, impact testing and ambient vibration are some of the more popular methods of dynamic testing. Forced vibration is a technique in which a sinusoidal force is applied to a structure in a varying frequency sweep. Impact testing is a technique in which an instantaneous force is applied in the form of a single impact and the resulting behaviors are recorded. Ambient vibration testing is simply recording the behavior of a structure when excited by the surrounding environment.

Until the late 1970's most of the full-scale field tests being conducted were static in nature. While static tests are sufficient in determining flexural capacities they fail to determine such characteristics as stiffness and responses to strong ground motion (earthquakes). Dynamic properties of structures include, but are not limited to, natural frequencies, mode shapes, modal stiffness and modal damping. Dynamic tests are used to determine such structural characteristics. Conducting dynamic tests and analyzing the results to make conclusions is known as structural identification. The structural identification concept was first introduced by Liu and Yao in 1978. Structural identification has been defined as the art of analytically conceptualizing, modeling, measuring, and quantifying structural behavior as well as the phenomena affecting it, in order to make engineering decisions (Aktan, 1997).

Dynamic testing has been used for many years to characterize and determine the structural integrity of a structure (Aktan et al, 1997, Liu 1995, Muhammad et al. 1999, Pandey et al. 1991, Salawu and Williams 1995). Although the concept of structural identification is not a new one, dynamic testing results from full-scale civil engineering structures are still few (Salawu and Williams, 1995). Experimental results from full-scale dynamic testing are even fewer with respect to condition assessment. Therefore, it is important to the future of structural earthquake engineering to be able to conduct full-scale dynamic testing in regards to condition assessment. Condition assessment is the science of determining how changes in structural parameters affect the dynamic characteristics of a structure. According to Muhammad et al. (Muhammad et al, 1999), changes in parameters such as stiffness, mass and damping lead to changes in dynamic characteristics such as natural frequencies, mode shapes, and modal damping.

The recent redesign and reconstruction of the I-15 corridor through Salt Lake City provided researchers at Utah State University with several full-scale bridges and bridge components ideal for condition assessment research. The bents selected for this portion of the research represent full-scale bridge components. Each of the three bents tested was subjected to two independent, separate states of damage after being tested in an undamaged state. Each state of damage was localized, severe, and well documented. Conclusions from this research project will indicate if forced-vibration testing used with modal analysis is an acceptable approach to damage detection. Additionally, the ability to construct discrete finite element models that closely match the field results will be investigated. The results from the testing of these bents are important for several reasons. First, the structures are full-scale and on location, this provides for real-world boundary conditions that cannot be matched in the laboratory, such as soil-structure interaction. Second, the deck has been removed leaving three separate structures that are relatively simple to model. Third, because the structures are very similar, conclusions may be drawn as to the repeatability of the tests. Fourth, these structures have been in service for more than 30 years and they represent mature, baseline structures.

2.2 EXPERIMENTAL METHODOLOGY

2.2.1 Test structures

Three reinforced concrete bridge bents that served as part of the 600 viaduct in Salt Lake City served as the test specimens. The three adjacent bents were left standing and intact after the deck had been removed. All three bents were similar in condition having experienced a moderate amount of spalling on the underside of the bent caps and minor cracking throughout. The bents were identical in their geometry and reinforcement, they differed only in elevation. The bents were 16.46 m (54 ft) long and 0.914 m (3 ft) wide. The bent cap was 1.52 m (5 ft) deep supported by two rectangular columns 0.914 m (3 ft) by 1.07 m (3.5 ft). The columns were spaced 10.36 m (34 ft) between centerlines. Beyond the outside edge of the columns, the depth of the beams tapered to 0.69 m (2 ft) over a length of 2.51 m (8.25 ft). Figures 2.1 and 2.2 show the general geometry of the bridge bents.

For research purposes, the bents were numbered from one to three, where bent one was the middle bent, bent two was the westernmost bent and bent three was the easternmost bent. The bents were numbered

in this fashion to reduce the possibility of future confusion because the middle bent was the first one to be tested for accessibility reasons. Other than a slight variation in height, the bents were geometrically identical. Bent one was 7.16 m (23.5 ft) in height from the pile cap to the bottom of the bent cap, bent two was 7.31 m (24 ft) in height and bent three was 7 m (23 ft) in height. The bents were supported on deep foundations consisting of six piles per column.

2.2.2 The eccentric mass shaker and instrumentation

The forced vibration was achieved with the use of an eccentric mass shaker. The shaker exerts a sinusoidal force in any horizontal direction as determined by the operator. The force is exerted by eccentric weights on two spindles at some distance *r*, rotating in opposite directions. The magnitude of the force can be adjusted by simply changing the eccentricity of the weights. The forcing has an upper limit of 89 kN (20,000 lbf) (Muhammad et al. 1999). The shaker was mounted to the bent cap via anchor bolts set about the perimeter of the machine. The anchor bolts were set 25 to 30 cm (10 to 12 inches) into the concrete with epoxy. The location of the shaker on the bent cap is shown in Figure 2.1.

Discrete instrumentation of the bents was difficult because of the limited number of instruments (nine). The bents were instrumented with force-balance accelerometers. Seven of the nine accelerometers had a limiting range of 1g while the other two had a limiting range of 0.25g. The 0.25g instruments were always placed in a horizontal direction. Each bent was instrumented a little differently than the next to try and determine the behavior at varying locations on the structure. For example, bent one was instrumented with seven instruments along the top of the bent cap, five accelerometers in the transverse direction and two in the longitudinal direction. One more accelerometer was placed in the vertical position on the outside edge of each column 3.96 m (13 ft) below the bent cap, to determine the rocking motion of the bent. Bent two was instrumented with six accelerometers along the top, four in the transverse direction and two in the longitudinal direction. The three remaining accelerometers were placed directly on the pile cap of the south column in the transverse, longitudinal and vertical directions. The objective of this was to characterize the behavior of the soil-structure interface. Bent three was instrumented identically to bent two on the bent cap. The three remaining accelerometers were placed on the column just above the pile cap in the transverse, longitudinal and vertical directions. Each accelerometer is capable of either a horizontal or a vertical orientation. For consistency, all horizontal accelerometers were positioned such that they measured positive accelerations in either the global North or East directions. The vertical accelerometers measured positive accelerations in the up direction.

Each accelerometer was mounted on a bent using a 152.4mm (6 in) square steel plate with cap screws. The plate was then attached to the bent at its respective location using three expansion anchors. This method of mounting accelerometers ensures that each instrument is level and consistent from test to test. Care was taken to ensure that the same instruments were always used at the same locations on any one bent for consistency in data acquisition. Furthermore, the same cables were always used with the same instruments. The natural frequencies and the associated mode shapes for each bent were determined by only using the channels on the bent caps. The comparisons made between the displacement mode shapes of the field data and the displacement mode shapes of the models were described by considering only the bent cap channels. Therefore, Figure 2.1 shows only the instrument layout on the bent cap with the arrow denoting the positive direction.

2.2.3 Condition assessment testing procedures

Each of the three bents was tested three times for a total of nine complete tests. Each bent was tested in an undamaged state followed by two additional tests at various levels of damage.

2.2.4 State 1-undamaged

To form a baseline for the test results each of the three bents were initially tested in an undamaged state. The testing procedure used was a horizontal sine sweep ranging from 1.0 Hz to 20 Hz in increments of 0.05 Hz at 20 seconds for each increment. The first four dynamic modes of the structure were excited in this range of frequencies. Because the force exerted by the shaker is a function of the frequency and the eccentricity of the weights, the eccentricity had to be reduced at 10 Hz to limit the structural response to within the range of the accelerometers. The shaker ran at 100 percent eccentricity from 1 to 10 Hz and typically at 30 percent from 10 to 20 Hz. The alignment of the eccentric weights exerted a sinusoidal force at a 45-degree orientation to the structure. Exerting the force at 45 degrees ensured that both the longitudinal and the transverse modes would be excited.

2.2.5 State 2-damage at each bent

When the baseline for each structure had been determined, the first state of structural damage was inflicted. For bent 1, the first state of damage included removing a significant amount of concrete from the top of the North column just below the bent cap. The first state of damage at bent 2 included removing approximately one-third of the pile cap from the South column and removing two of the piles from the structural system. The first state of damage at bent 3 included removing approximately one-sixth of the pile cap from the South column and removing one pile from the structural system. Upon completion of the damage, the horizontal sine sweep was re-administered. Instrumentation and techniques were kept consistent with the undamaged test

2.2.6 State 3-additional damage at each bent

After the second state of the structure had been tested, additional damage was inflicted to each bent. The second state of damage at bent 1 included inducing more damage at the top of the North column. During this stage nearly all of the perimeter reinforcement had been severed and the amount of concrete removed doubled. The second state of damage at bent 2 included removing nearly one-fourth of the pile cap at the North column and removing one pile from the structural system. The second state of damage at bent 3 included removing a large quantity of concrete and severing several longitudinal reinforcement bars at the base of the South column just above the pile cap. Upon completion of this stage of damage, the horizontal sine sweep was administered exactly as it was in the previous two tests. Figure 2.2 shows the severity and location of the damage states for each bent. Figure 2.3 is a photograph showing typical foundation and pile damage. This particular photo looks down at the pile cap where a pile has been removed from the superstructure. The soil was replaced immediately following the damage. This photo shows one of the two piles that were removed for state 2 of bent 2. Figures 2.4(a), 2.4(b) and 2.4(c) are photographs showing the condition at the North column of bent 1 for state 1, 2 and 3.

2.3 FINITE ELEMENT MODELING

Detailed finite element models were created for each bent. A structural engineering modeling and design software, SAP 2000, was used to create the models. The superstructure was modeled using beam-column elements. All elements of the superstructure were modeled as concrete with the same dimensions as the full-scale structure. The cantilevers of the bent caps were modeled using 11 elements, each having a length of 228mm (9 in). The beams were modeled using 75 elements, each having a length of 152.4mm (6 in). The columns were also modeled using beam-column elements, each having a length of 152.4mm (6 in). The number of column elements varied from bent to bent to accommodate the elevation differences.

In an attempt to best replicate the boundary conditions found in the field, the foundations of the bents were modeled as solid concrete elements to the exact dimensions. Solid elements have no rotational degrees of freedom, therefore the solid elements were analyzed according to the assumption that the pile cap acts as a rigid body. The piles were modeled as individual springs attached to the pile cap at each respective location. For each pile two springs were assigned, one in the longitudinal direction and one in the transverse direction. A roller was attached at each pile location to accommodate for the vertical reactions.

A separate model was produced for each damage state. The models were created to correlate with the actual damage induced at each bent. To model the column damage, cross-sectional areas of the column elements in the model were reduced to best match the reduction in cross-sectional area at the same location on the structure. This technique reduced the moment of inertia of the model the same as the damage for the bent. Foundation damage was modeled by removing solid elements equal to approximately the same volume and location as the bent damage. If a pile had been removed, the springs at that location were simply removed.

2.4 DATA ANALYSIS AND RESULTS

2.4.1 Field data analysis

Conducting the fieldwork for this research took approximately one month to complete. The process of obtaining the dynamic characteristics of the structures from nine files of raw data was next. The raw voltage data obtained from the accelerometers was contaminated with noise. The primary step in data analysis was to extract the clean voltage signal from the noisy signal. Cleaning the signal was accomplished with a technique referred to as demodulation (Bay 1997, Halling et al. 1999b).

Demodulating the data commenced by calculating an average frequency for which the shaker was running over a given 20 second data collection block. All channels recording responses were compared to the average frequency of the shaker channel. Every data point in the signal of every channel was analyzed. If any data point was within +/- 5 percent of the average frequency of the shaker, that point was retained. If any data point was outside the +/- 5 percent range, that data point was discarded. The data signal is a sinusoidal curve that can be characterized by its amplitude and phase. The values

obtained for amplitude and phase were converted to displacement per unit force and phase angle relative to the machine channel. To convert to the relative phase angle, the absolute phase of the shaker was subtracted from the absolute phase of each channel.

In the analysis the converted displacements per unit force were plotted in the frequency domain. The original field data had been recorded in frequency blocks in increments of 0.05 Hz. To pinpoint natural frequencies at increments smaller than 0.05 Hz, a cubic spline interpolation was used to interpolate between data points. A cubic spline interpolation fits a third order polynomial between every two data points with different specific constraints at each point. Accurate frequency values were then determined on the order of 0.005 Hz.

The natural frequencies of the field structures were reduced with each state of damage, which is consistent with a reduction in structural stiffness. One exception is mode four of bent two, which had an increase in natural frequency from state 1 to state 2, which is apparently the result of experimental error. When the displacement values had been determined and the relative phase angles had been calculated, the mode shapes correlating to the natural frequencies were plotted. Figure 2.5 shows the first four typical mode shapes for the field structures and the finite element models.

2.4.2 Model analysis

As previously stated, a series of finite element models were created with the SAP 2000 finite element analysis software program to best replicate the results of the field data. To correctly match the data, the springs at the pile locations had to be assigned accurate constants. Several estimates were made as to the range of acceptable spring constants. The range of spring constants were optimized with an iterative optimization algorithm and the best-fit parameters were determined (Halling et al. 1999b).

Once the spring constants were determined, the first three natural frequencies of each bent for state 1 matched closely with the field results. To further increase the accuracy of the state 1 frequencies, moments of inertia of model elements were altered to increase or decrease their stiffness. For the bent 1 model, the moment of inertia of the top beam about a vertical axis was multiplied by a factor of 1.3. Use of this factor increases the stiffness in the transverse direction to increase the natural frequency of the fourth mode to match almost exactly with the field data. Moments of inertia of model elements for bents 2 and 3 were also altered until their natural frequencies matched closely with the field data. Once the state 1 frequencies had been matched, all spring constants and moment of inertia factors remained constant from state to state. The only changes made to the models were those directly related to the damage states. Tables 2.1(a) and 2.1(b) summarize the natural frequencies for each state of each mode of each bent between the model and the field. Ratios are shown to give some idea as to the amount of change in frequency. In Table 2.1(c), a value of unity means the natural frequency of the model matches exactly with the natural frequency of the field data. The first four mode shapes of the models are similar to those of the bents and are shown in Figure 2.5.

2.5 CONCLUSIONS AND RECOMMENDATIONS

Upon completion of the forced vibration testing and the data analysis and the subsequent finite element modeling of three full-scale reinforced concrete bridge bents several important conclusions may be drawn. The damage inflicted on the structures was detectable by noting the changes in the natural frequencies and mode shapes. Furthermore, when the model was changed in a way that closely matched the damage to the bent, the changes in the model mode shapes were indicative of the changes noted in the field data. These changes are a direct result of the reduction in structural stiffness.

It is recommended that the use of more instrumentation be investigated, especially at the foundation level, to better characterize the soil-structure interface. More instrumentation could have been placed at discrete intervals along the beam and columns to investigate the significance of elastic deformation.

The finite element models constructed and analyzed here proved to be sufficient in matching the field results in the first state. However, more research is required to determine how to best model the damage and foundation system. The models describing the second and third states of damage did not differ from the baseline model as significantly as the corresponding states of the bents differed from the baseline data. This may be due, in part, to the disruption of the soil surrounding the bents while damaging the foundation system.

TABLE 2.1(a). Natural frequencies and ratios for field data.

BENT 1	state 1	state 2	state 3	state 2/state 1	state 3/state 2	state 3/state 1
mode 1	3.700	3.695	3.635	0.9986	0.9838	0.9824
mode 2	6.460	6.255	6.080	0.9683	0.9720	0.9412
mode 3	7.375	6.985	6.695	0.9471	0.9585	0.9078
mode 4	15.390	14.915	14.910	0.9691	0.9997	0.9688
BENT 2	state 1	state 2	state 3	state 2/state 1	state 3/state 2	state 3/state 1
mode 1	3.480	3.340	3.270	0.9598	0.9790	0.9397
mode 2	6.105	5.790	5.700	0.9484	0.9845	0.9337
mode 3	6.745	6.160	5.940	0.9133	0.9643	0.8807
mode 4	14.865	15.085	15.010	1.0148	0.9950	1.0098
BENT 3	state 1	state 2	state 3	state 2/state 1	state 3/state 2	state 3/state 1
mode 1	3.730	3.650	3.490	0.9786	0.9562	0.9357
mode 2	6.535	6.370	6.215	0.9748	0.9757	0.9510
mode 3	7.465	7.155	6.945	0.9585	0.9706	0.9303
mode 4	15.550	15.500	15.410	0.9968	0.9942	0.9910

TABLE 2.1(b). Natural frequencies and ratios for finite element models

BENT 1	state 1	State 2	state 3	state 2/state 1	state 3/state 2	state 3/state 1
mode 1	3.766	3.755	3.736	0.9971	0.9949	0.9920
mode 2	6.418 Hz	6.357 Hz	6.349 Hz	0.9905	0.9987	0.9892
mode 3	7.380	7.225	7.231	0.9790	1.0008	0.9798
mode 4	15.337	15.198	15.152	0.9909	0.9970	0.9879
BENT 2	state 1	State 2	state 3	state 2/state 1	state 3/state 2	state 3/state 1
mode 1	3.494	3.438	3.413	0.9840	0.9927	0.9768
mode 2	5.956	5.627	5.525	0.9448	0.9819	0.9276
mode 3	6.729	6.447	6.353	0.9581	0.9854	0.9441
mode 4	14.881	14.472	14.368	0.9725	0.9928	0.9655
BENT 3	state 1	State 2	state 3	state 2/state 1	state 3/state 2	state 3/state 1
mode 1	3.795	3.779	3.621	0.9958	0.9582	0.9542
mode 2	6.510	6.489	6.266	0.9968	0.9656	0.9625
mode 3	7.474	7.457	6.784	0.9977	0.9097	0.9077
mode 4	15.576	15.601	15.385	1.0016	0.9862	0.9877

TABLE 2.1(c). Field data natural frequencies over model natural frequencies.

BENT 1	state 1/state1	state 2/state 2	state 3/state 3
mode 1	0.9825	0.9840	0.9730
mode 2	1.0065	0.9840	0.9576
mode 3	0.9993	0.9668	0.9259
mode 4	1.0035	0.9814	0.9840
BENT 2	state 1/state1	state 2/state 2	state 3/state 3
mode 1	0.9960	0.9715	0.9581
mode 2	1.0250	1.0290	1.0317
mode 3	1.0024	0.9555	0.9350
mode 4	0.9989	1.0424	1.0447
BENT 3	state 1/state1	state 2/state 2	state 3/state 3
mode 1	0.9829	0.9659	0.9638
mode 2	1.0038	0.9817	0.9919
mode 3	0.9988	0.9595	1.0237
mode 4	0.9983	0.9935	1.0016

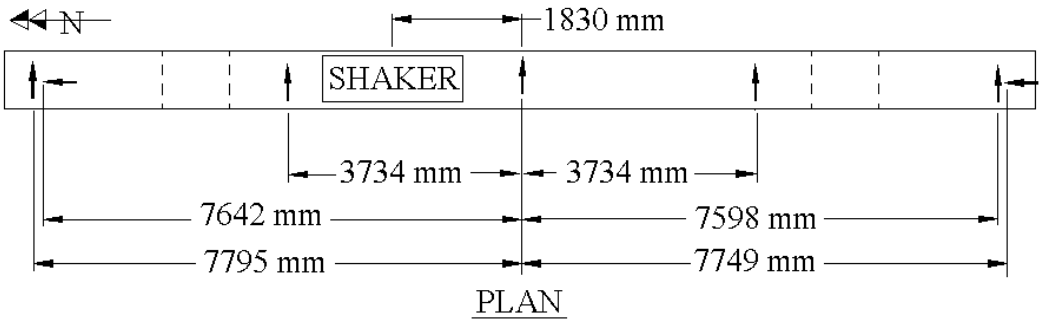

Figure 2.1. Instrumentation and shaker location.

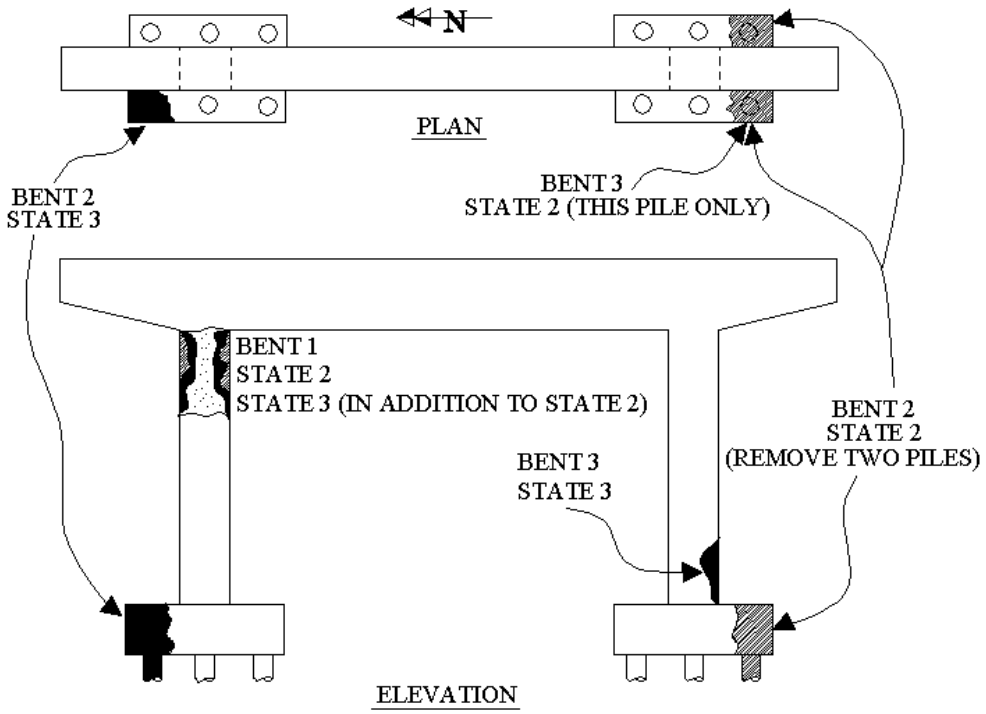

Figure 2.2. Schematic showing damage severity and location for states 2 and 3.

Figure 2.3. Typical foundation and pile damage

Figure 2.4(a). Condition of North column of bent 1 at state 1 (undamaged).

Figure 2.4(b). Condition of North column of bent 1 at state 2.

Figure 2.4(c). Condition of North column of bent 1 at state 3.

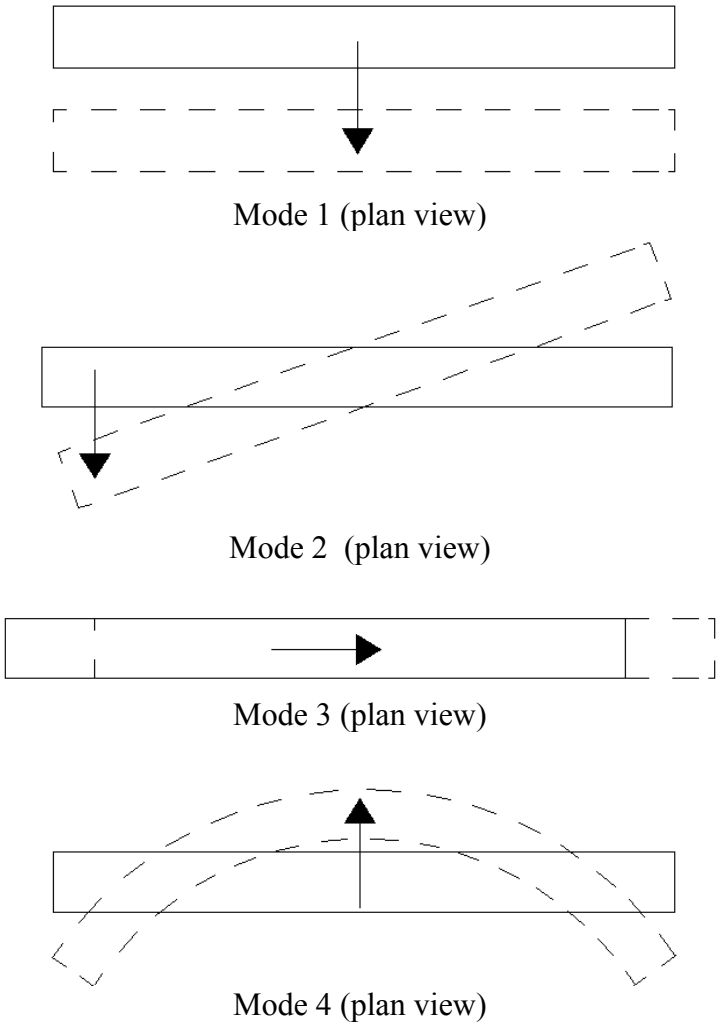

Figure 2.5. Typical mode shapes from the field data and finite element models.

CHAPTER 3

Six-span bridge at 500 South

Forced vibration testing of a full-scale, reinforced concrete bridge was performed by researchers from Utah State University. As part of the reconstruction of I-15 through Salt Lake City, several bridge structures planned for demolition were made available for testing. One of these structures prepared for demolition was a six span bridge that was used for the testing described in this chapter. The bridge was tested in four different condition states for which damage was inflicted upon the bridge at a different location for each testing state. These tests were performed to characterize the bridge based on its modal parameters. In addition to characterizing the bridge, the testing was performed to determine any correlation between the modal parameters of the bridge and the location of the inflicted damage. An eccentric mass shaker was used to excite the test structure for which the response of the bridge was recorded by an array of seismometers. The response data was processed to determine the modal frequencies, and mode shapes of the bridge. There were noticeable variations in the modal frequencies and mode shapes for each testing condition. These results were used to construct optimized finite element models of the bridge. These finite element models were used for damage detection in the bridge using various methods.

3.1 INTRODUCTION

The concept of dynamic testing to assess the condition of large structures, commonly referred to by some as Structural Identification (ST-Id) was first introduced by Liu and Yao in 1978. Since this time many researchers, using different methods, have followed Liu and Yao's concept of Structural Identification. Still more testing is necessary to determine the feasibility of assessing the condition of bridges and other civil structures through the use of forced vibration monitoring.

Global modal parameters, such as modal frequencies, modal damping, and mode shapes, can be used to assess the internal properties or condition of a structure. These modal parameters are a function of the physical parameters, stiffness, mass, and damping, of a structure. Knowing that damage to a structure will alter the physical parameters of a structure, a change in the global modal parameters of the structure would also be expected. It also holds true that each mode of vibration (modal frequency) has a different energy distribution. As a result of this energy distribution the location as well as magnitude of localized damage will affect each mode differently, Salawu and Williams (1995). In theory this would allow the location of damage to a structure to be identified based on observed changes in the modal parameters.

Forced vibration testing was performed prior to and following four damage states inflicted at different locations of a six span full-scale bridge. A decrease in the modal frequencies as well as changes in the mode shapes of the structure noted a reduction in stiffness of the structure as a result of localized damage. A testing methodology, as well as analysis results, are presented in this chapter. The results

from the modal analysis were used in constructing optimized finite element models of the bridge. These models were then used for damage detection using concepts like Center of Rotation and MAC and COMAC. These results and conclusions are also presented.

3.2 TESTING METHODOLOGY

The 5th South viaduct in Salt Lake City was demolished at each end leaving a six span freestanding bridge with no boundary constraints at the ends. Each of the six spans as well as the seven bents that supported the spans were identical in dimensions as well as construction, yielding a symmetric test structure. Each span was 18.3m (60ft) long by 16.8m (55ft) wide. The deck was constructed of reinforced concrete, and was supported by seven pre-stressed concrete beams. The beams rested on 25mm (1in) thick neoprene bearings that were located on the bent caps. The bents were also constructed of reinforced concrete and were supported by a pile group under each column. A detailed drawing of the bridge with dimensions as well as a numbering system for bridge bents and deck spans that will be referred to later can be seen in Figure 3.1.

3.3 INSTRUMENTATION

The bridge was instrumented with 30 horizontal seismometers and six vertical seismometers. The scope of this chapter is limited to the 18 horizontal seismometers located on the deck of the bridge.

3.3.1 Instrumentation Setup

Working with a limited number of seismometers, an instrument layout schematic was formulated to capture what was deemed to be the most valuable points of the structure to best describe the transverse and longitudinal mode shapes. Each span of the bridge was instrumented with three horizontal instruments. Of these three instruments, two were oriented transverse to the bridge, and one was oriented longitudinal to the bridge. Each instrument was located equidistant from the center of the span at a distance of 7.62m (25ft). Assuming each span to behave as a rigid body, this setup allowed for the translation as well as rotation of each span to be calculated. See Figure 3.2.

3.3.2 Damage States

The bridge was tested at a total of four different condition states. The first condition state was with the bridge in its undamaged state. The collected data from this test served as a baseline for which all other testing states were compared. The second testing state consisted of damage inflicted at the base of the South column of bent 2. Approximately one fourth of the cross section of the column was removed exposing four sections of rebar. Two of these four sections of rebar were severed. The third state of damage was similar to the second state. For this testing state damage was inflicted to the base of the South column of bent 5. Approximately one third of the column cross section was removed. Four sections of rebar were exposed, three of which were severed. The final testing state consisted of disconnecting one pile from the North pile cap of bent 5. Due to the limitations of the equipment used,

all of the damage occurred at or below ground level. Each damage state was produced with the use of a backhoe and a pneumatic chisel. The location of each damage state can be seen in Figure 3.3.

3.3.3 Testing Procedure

For each damage state a test was conducted with the shaker machine located at each position A and B (see Figure 3.3), resulting in a total of 8 tests. For each test the eccentric mass shaker was set to force in the horizontal plane at an angle of 45 degrees to the axis of the bridge. This allowed the longitudinal as well as transverse modes of the bridge to be excited. Data was collected over a frequency sweep from 0.5 to 20hz at increments of 0.02hz. For each increment shift in the frequency, the structure was allowed to reach steady state at which point data was acquired for approximately 20 seconds at a sampling rate of 100 samples per second. Each test required approximately eight hours to complete.

3.4 DATA PROCESSING AND ANALYSIS

Following testing, the collected data was processed to extract an amplitude response as well as a phase angle for each seismometer. From the amplitude response and phase angle of each seismometer the modal frequencies, and mode shapes were calculated.

3.4.1 Data Processing

The data was processed using a method referred to as demodulation. The forcing produced by the eccentric mass shaker can be described by

$$F=mr\omega^2 \sin\omega t \tag{3.1}$$

where m is the mass of the rotating weights, r is the radius, t is the time, and ω is the angular velocity at which the weights are spinning. As can be seen, the forcing is a function of the frequency at which the shaker operates. Therefore, the bridge displacements were normalized by the excitation force, resulting in displacements per unit force.

Following the processing of the acquired data, the amplitude response (Figure 3.4) and phase angle were plotted against the frequency of excitation to produce amplitude response and phase angle spectra. To increase resolution a cubic spline was fit to the data.

3.4.2 Modal Frequencies

The modal frequencies were determined from the displacement amplitude plots. Each peak in the curve (Figure 3.4) corresponds with a modal frequency. The modal frequencies, with the shaker at location A, for the first seven modes can be seen in Table 3.1. Mode 1 is the first longitudinal mode of the structure

and modes 2 through 7 are transverse modes. The modal frequencies obtained with the shaker machine located at position B were very similar to those obtained with the shaker at position A.

TABLE 3.1 Modal Frequencies For First Seven Modes at Four Damage States (Shaker Position A)

Mode	State 1	State 2	State 3	State 4
1	1.170 Hz	1.118 Hz	1.102 Hz	1.096 Hz
2	2.292 Hz	2.272Hz	2.265 Hz	2.256Hz
3	2.540 Hz	2.450 Hz	2.457 Hz	2.445 Hz
4	2.892 Hz	2.824 Hz	2.826 Hz	2.809 Hz
5	3.756 Hz	3.338 Hz	3.379 Hz	3.345 Hz
6	4.834 Hz	3.978 Hz	4.129 Hz	3.960 Hz
7	5.736Hz	5.011 Hz	5.660 Hz	5.247 Hz

It is interesting to note that for many of the modes there is an increase in frequency from state 2 to state 3. This is contradictory of what would normally be expected. With the increased damage from state 2 to state 3 it would be expected that there would be a decrease in the modal frequency. Other than this discrepancy from state 2 to state 3 there was a consistent decrease in the modal frequency as a result of damage to the structure.

3.4.3 Mode Shapes

Mode shapes for each mode were obtained from the amplitude of each seismometer at a modal frequency with the accompanying relative phase of each seismometer. For the first longitudinal mode, only the seismometers oriented in the longitudinal direction were considered. In a similar manner for the transverse modes only the seismometers oriented in the transverse direction were considered. Seismometers exhibiting a phase near +90 were assumed to be displaced to the North, and seismometers exhibiting a phase near –90 were assumed to be displaced to the South. Using these assumptions the mode shapes for modes 2 through 6 were plotted for machine position A at all four condition states. These mode shapes can be seen in Figure 3.5.

In Figure 3.5, the first six transverse mode shapes of the structure can be seen. Each plot shows the change in the mode shape for each condition state. The mode shapes for the machine at position B are very similar for those of position A. It can be seen from these plots that the frequency is inversely proportional to the amplitude of displacement. This is especially noticeable in modes 6 and 7 where the amplitude of state 2 is significantly greater than states 1, 3, and 4.

As the stiffness of the structure (k) decreases, the same forcing is applied, and there is no change in the mass (m), there will be an increase in the amplitude and a decrease in the natural frequency $\omega_{n.}$. For modes 5, 6, and 7 it is seen that the seismometers located at the joints between spans are not always in phase with one another. This can be explained by the neoprene bearings that allow the spans to move in opposite directions to fit higher mode shapes. It is yet unknown the full extent that the neoprene bearings may have on the mode shapes of this structure.

3.5 FINITE ELEMENT MODELLING

3.5.1 Model Description

Different finite element models of varying degrees of complexity were constructed using SAP2000 finite element analysis software. The columns, girders and the piles of the finite element model were modeled using frame elements. The piles were assumed fixed several feet below the ground level. This depth to fixity was later determined through an optimization procedure. The pile cap itself was modeled using rigid links from the base of the column to the piles. The concrete deck was modeled using thin shell elements. The deck was assumed to be rigidly connected to the girders. The vertical springs (springs in the z direction) were considered to be very stiff in comparison to the horizontal springs and their stiffness was therefore set to a very high value.

The final finite element model of the bridge is shown in Figure 3.6. The pile cap at the base of the columns was about 1.07m (3.51 ft) thick and was therefore considered to be a rigid body. Hence, it was modeled using rigid links from the base of the column to piles. The piles were assumed fixed at a certain depth below the ground level. It should be noted that in this analysis, only the modal frequencies were considered as the criteria for judging the accuracy of the finite element model.

3.5.2 Optimization

The aim of this optimization was to arrive at the values of the parameters, so as to match the natural frequencies of the bridge as closely as possible. The parameters in this problem were the values of the stiffness of the springs used in the neoprene bearings, the depth to fixity of the pile group, and the modulus of elasticity of concrete.

The ideal optimization algorithm would go through all the possible values of the parameters and try all possible combinations and pick up the one combination that would get the error to the least possible value. However, trying all possible combinations on a finite element model is practically impossible. Instead, the finite element model was itself reduced to a mathematical form (Quasi-structural model) using the method proposed by Douglas and Reid (1982). This Quasi-structural model was then used in place of the finite element model for the optimization process.

After the finite element model was optimized for the undamaged state, it was damaged in exactly the same locations as the bridge and the frequencies of the modes are compared in Table 3.2.

TABLE 3.2 Modal Frequencies (Field Values and Damaged Model Values)

		Mode 1 (Hz)	Mode 2 (Hz)	Mode 3 (Hz)	Mode 4 (Hz)	Mode 5 (Hz)	Mode 6 (Hz)
State 1	Model	1.280	2.523	2.703	3.032	3.486	4.132
	Field	1.175	2.280	2.535	2.918	3.730	4.658
State 2	Model	1.255	2.512	2.682	3.019	3.482	4.124
	Field	1.118	2.261	2.458	2.841	3.281	4.003
State 3	Model	1.249	2.500	2.686	3.027	3.471	4.127
	Field	1.102	2.258	2.471	2.834	3.296	4.099
State 4	Model	1.249	2.499	2.685	3.027	3.471	4.127
	Field	1.096	2.243	2.447	2.822	3.266	3.972

In general, the frequencies of a structure should decrease with damage due to softening of the structure. However, this was not observed in some cases in the field data as well as the finite element model results. As can be seen from the table above, the frequencies for modes three, five and six increased from damaged state one to damaged state two. The exact reason for these increases is not known and is probably due to computational or experimental errors. Such an increase was observed not with just these damage locations but also with other damage locations as well. The finite element model constructed was first subjected to the same damage levels, but at different locations as in the first damaged state of the actual structure. The effect of further damage at other locations on the frequency change was studied. The location of the first damage position was then changed and the above process repeated. No recognizable patterns were observed in these frequency shifts. These shifts could have been due to numerical errors in the software or due to minor changes in the nature of the mode shape itself that were not noticeable. The members were then made stronger, that is, their cross-sections were increased to see if such an effect could be seen. No such anomalies were observed.

3.6 DAMAGE DETECTION

As mentioned earlier, damage detection and serviceability assessment is a vital step in ensuring that a structure is effective for its intended purpose. This project was aimed towards studying and using these techniques to try and detect the damage inflicted on the bridge. The two major methods that were studied under this project were 1) The Center of Rotation technique and 2) The MAC-COMAC technique. The idea of Center of Rotation is taken from an earlier work by Muhammed, Halling, Womack (1999). The concept of MAC-COMAC (Lieven and Ewins, 1988) has been used in mechanical and aerospace applications for condition assessment for nearly 20 years. The feasibility of extending the same technique to full-scale civil engineering applications was studied. During the field-testing it was not possible to find the exact mode shapes of the bridge. Instead the response of the bridge at resonance was assumed to be a close approximation of its mode shape. In order to be consistent with this assumption, the finite element model of the bridge was excited with unit force that was applied so that it simulated the force exerted by the eccentric mass shaker. This dynamic response was taken to be the mode shape and was used in the center of rotation calculations.

3.6.1 Center of Rotation

The concept of center of rotation is based on the assumption that the deck of the bridge acts as a rigid body. Each of the deck segments was assumed to rotate about a point along the axis of the bridge (Figure 3.7). The centers of rotation of the decks were calculated before and after the model was subjected to damage. The displacements used in the center or rotation calculations were obtained by picking off the absolute maximun values of the displacements from the time history data of the model. Although some spans did show some changes in the centers of rotation for different damage states, nothing conclusive could be really said about them. The exact effect of the damage sequences on the centers of rotation is not known. Since this method of comparing the centers of rotation was not yielding consistant results, a different procedure was used to calculate the centers of rotation. In this method, the y components of the eigen vectors of the bents was used instead of the x displacements of the decks. The theory behind this method was that the bents were assumed to rotate about some center of rotation and that this center of rotation would change with damage (Figure 3.8).

A similar formula as the one obtained earlier for the span rotation was used here. The value of x (center of rotation) is given by

$$x = (d*Y_1)/(Y_1+Y_2)' \qquad (3.2)$$

where d is the distance between the two points where the eigen vectors were measured (Figure 3.8), and x is the distance to the center of rotation from the left point. The centers of rotation were calculated before and after the model was subjected to damage. The values of the centers of rotation for each bent for the transverse mode shapes in all the three damage-states and the original undamaged state were plotted together. These plots are presented in Figure 3.9. By looking at the center or rotation plots for the bents it can be seen that the bents with maximum displacement (in a particular mode shape) have maximum changes in their centers or rotation after damage. This effect is very clear in plots B and C. This effect with further study could be used as a method to at least indicate damage in the structure if not the damage location.

3.6.2 MAC and COMAC

The Modal Assurance Criterion or the MAC is loosely defined as “A scalar constant relating the casual relationship between two modal vectors”, (Lieven and Ewins, 1988). The eigen vectors for the first twenty mode shapes from the finite element model in its undamaged state and from the finite element models with various levels of damage were considered for this. This resulted in tables of MAC values with the leading diagonal elements close to one and the off-diagonal elements close to zero.

A MAC value of one indicates perfect correlation between the two mode shapes in the two data sets. The lower this MAC value, the lower this correlation. It was observed that the MAC values for modes three, four and five drop significantly when compared to other modes. This is an indication that the mode three and mode four in particular need not have the same modal properties in the first damaged state when compared to the undamaged state. In other words, what we think to be essentially the same

mode shape need not be the same. This difference although not obvious from the mode shapes themselves (displacement eigen values), is a possible cause for the random changes in the frequencies that were observed.

The MAC values only indicate the correlation between two modes but they do not give any indication of the co-ordinates or the locations of the nodes that are responsible for these differences. The Co-ordinate Modal Assurance Criterion or the COMAC, (Lieven and Ewins, 1988) seeks to identify the locations that are responsible for the deviations. Although changes were observed in COMAC values corresponding to the damage locations (nodes), the values at other locations also changed appreciably. The COMAC values changed from 0.99 to 0.96 at various nodes after damage state one. However since this change was not limited to damage locations alone, these numbers could not be used for damage detection.

3.7 CONCLUSIONS

Other than condition state 2, a decrease in modal frequency was observed for each damage inflicted on the bridge. This clearly indicated a softening of the structure. The mode shapes of the structure showed an increase in amplitude corresponding with the decrease in frequency for each damage state also indicating a reduction in stiffness. At this point it is difficult to determine the location of damage by observing the modes shapes. It appears that localized damage of the structure results in global changes to the structure. More testing is necessary to correlate global mode shape changes to localized damage.

The finite element model was dependent on the parameters described earlier and its accuracy in predicting the bridge response was improved by the optimization procedure. Damage detection using the center of rotation at deck level was inconclusive. The same theory when applied at the bent level showed some promising trends that need to be further investigated. It is highly recommended that MAC values be used as filters when comparing the mode shapes and frequencies between two states of damage. In other words, modes with lower MAC values may indicate different mode shapes. COMAC values were inconclusive at indicating damage. If these values are to be used for damage detection an alternate method of excitation is recommended. Unpredictable variations in the displacement patterns, especially around the source of excitation, were observed with the current method, which affected the COMAC values.

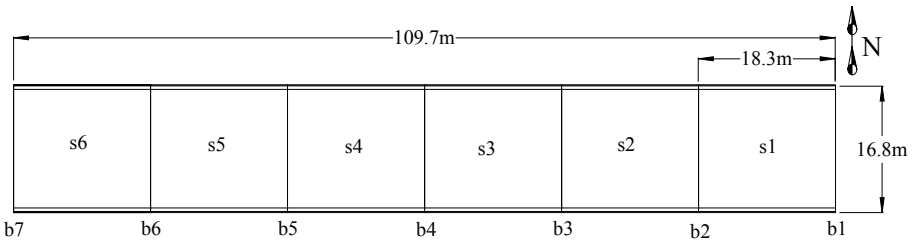

(a)

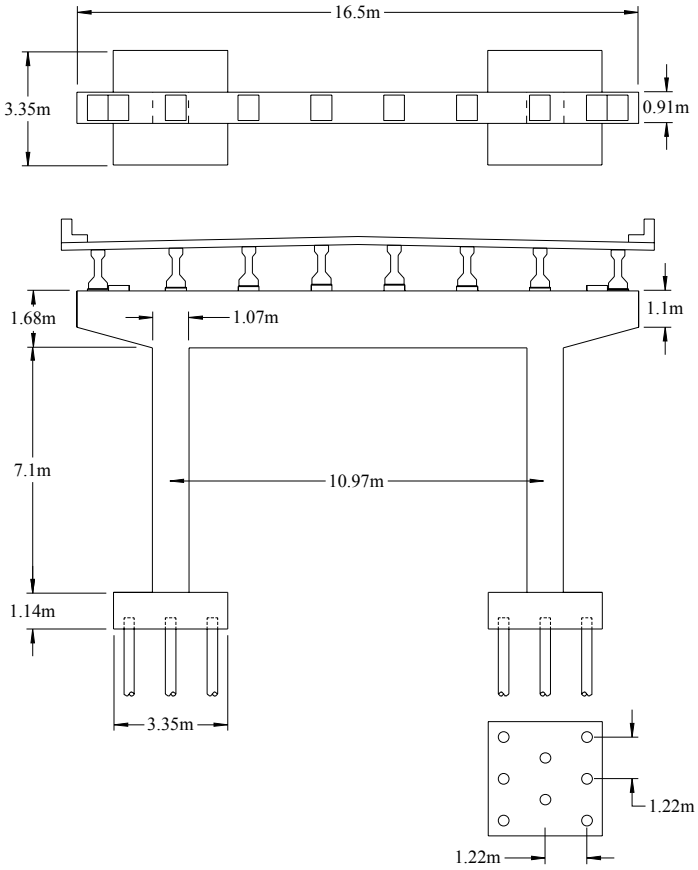

(b)

FIGURE 3.1 (a) Plan View of complete bridge. (b) Plan and elevation views of an individual bent.

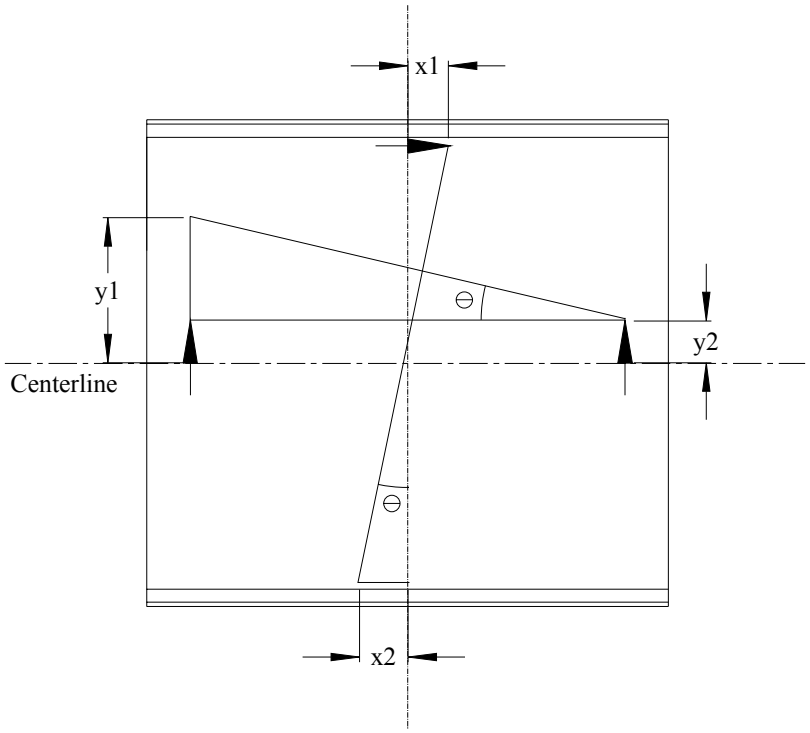

FIGURE 3.2 Illustration of seismometers (arrows) located on each bridge span. Illustration shows that the rotation and translation of each span can be determined by three seismometers.

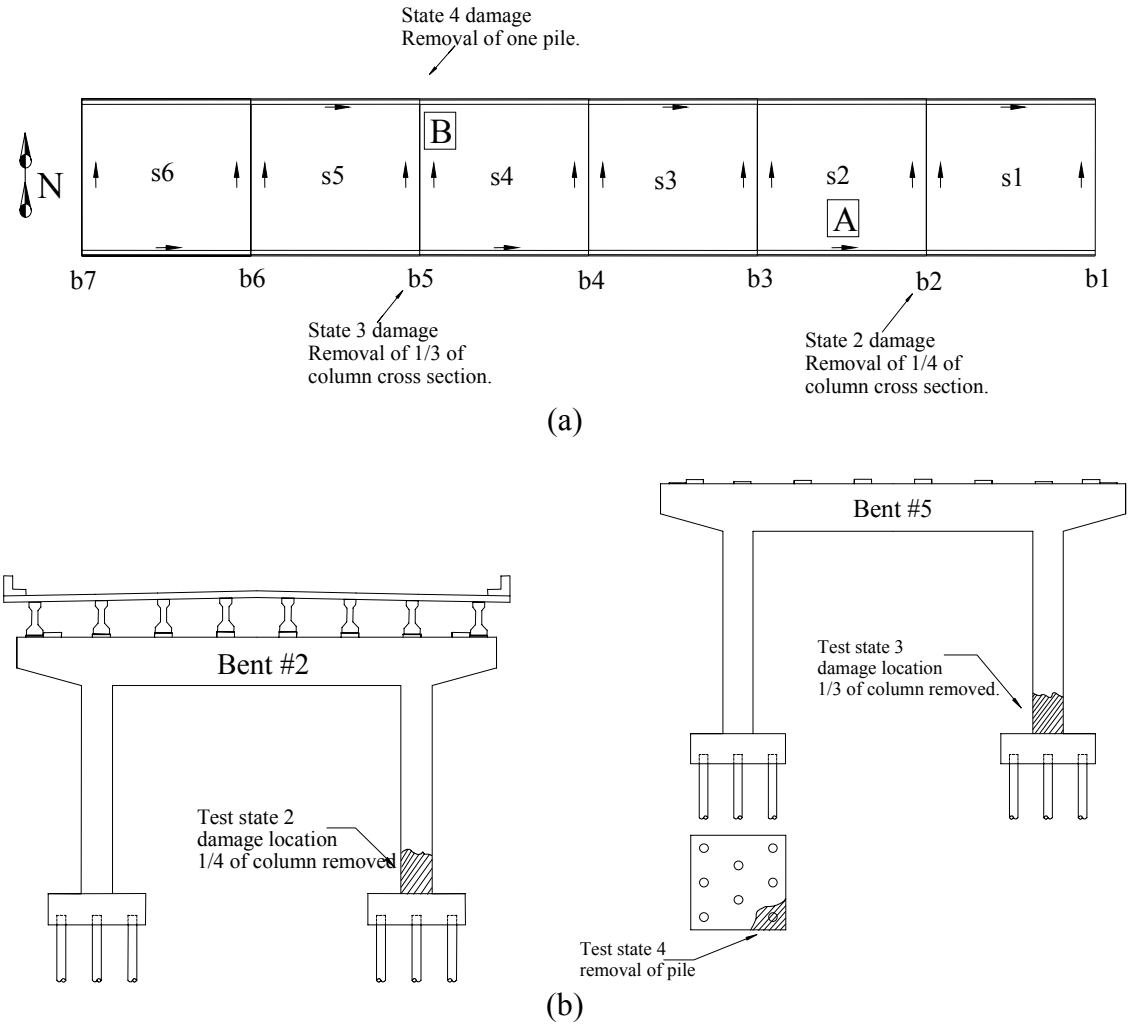

FIGURE 3.3 (a) Plan view showing global locations of damage as well as shaker and seismometer locations. (b) Detailed view of damage to bent 2 and bent 5.

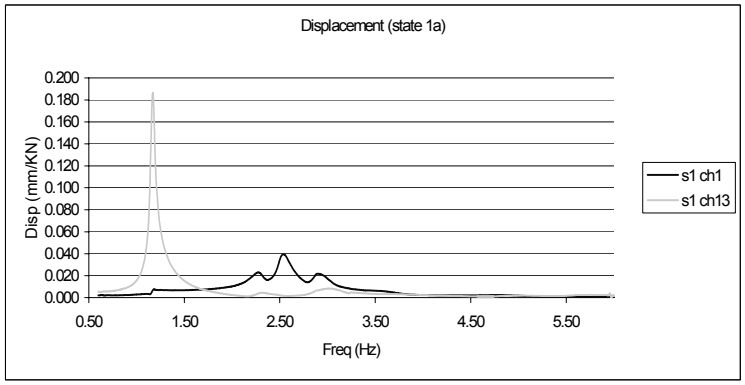

FIGURE 3.4 Plot of displacement vs. frequency.

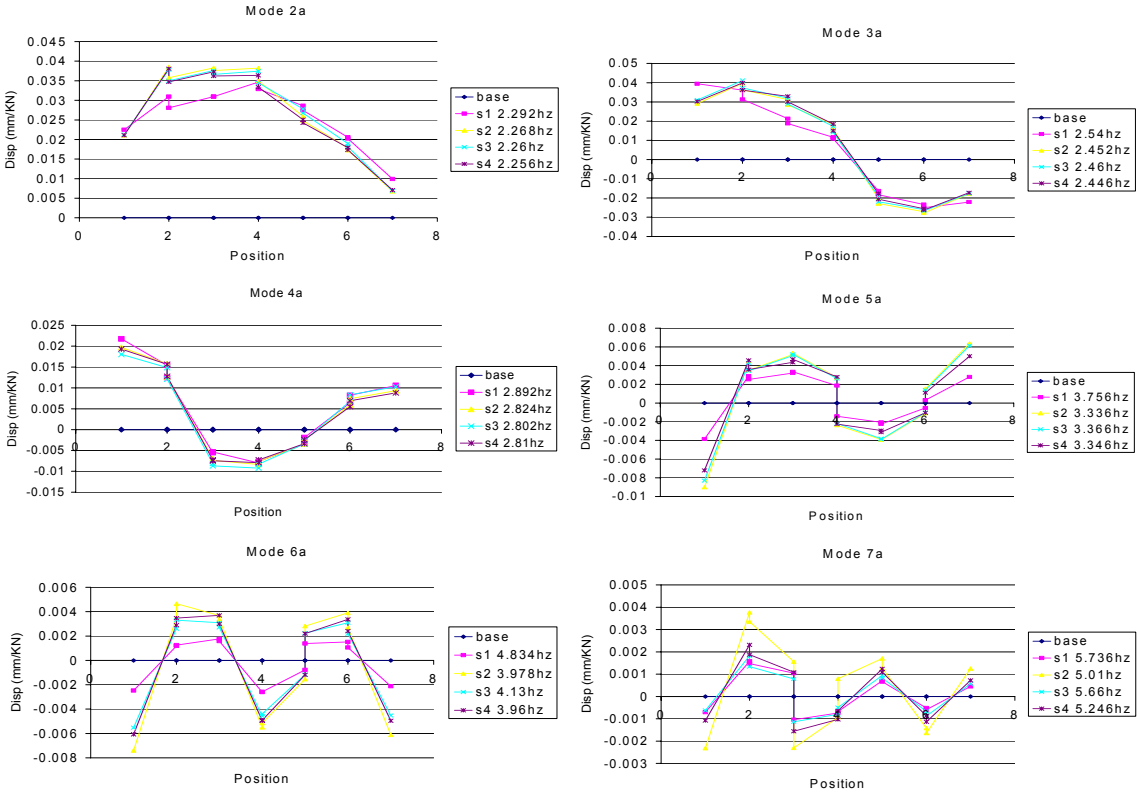

FIGURE 3.5 Transverse mode shapes for shaker in position A.

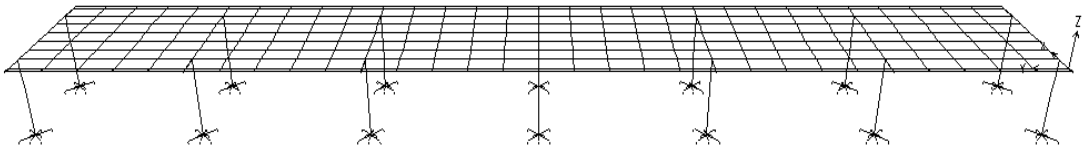

FIGURE 3.6 Finite element model – un-deformed geometry.

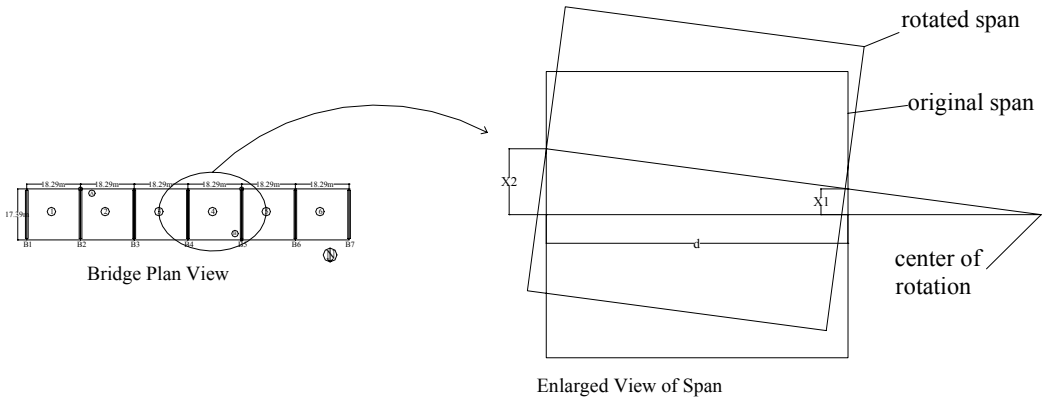

FIGURE 3.7 Center of rotation.

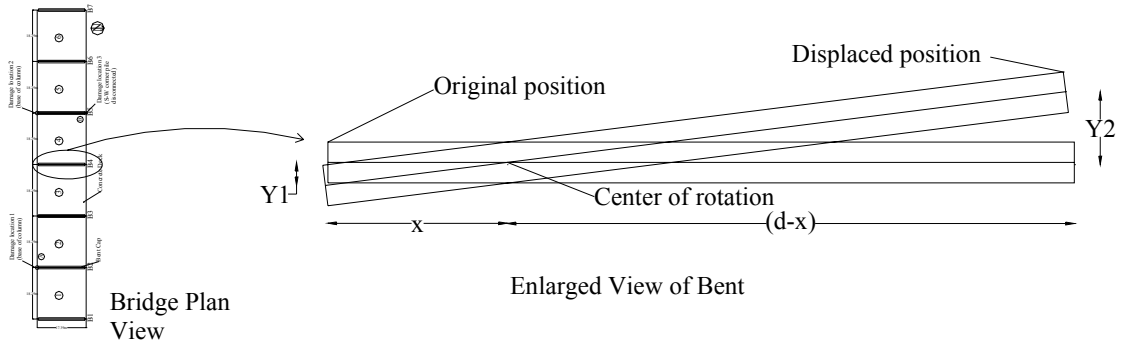

FIGURE 3.8 Bent rotation.

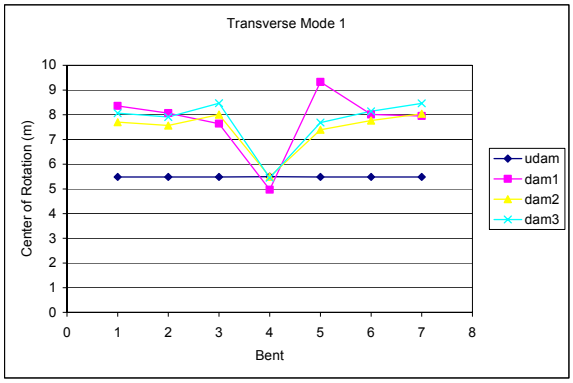

Plot A. Bent center of rotation transverse mode 1

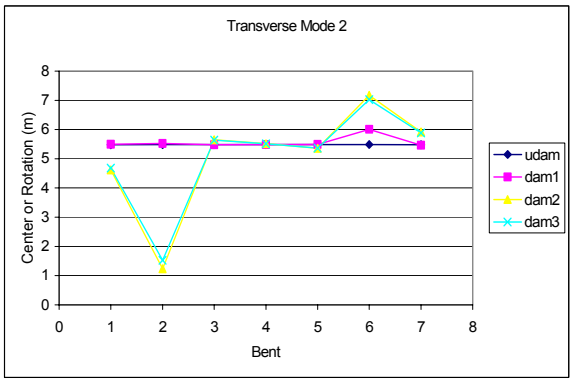

Plot B. Bent center of rotation transverse mode 2

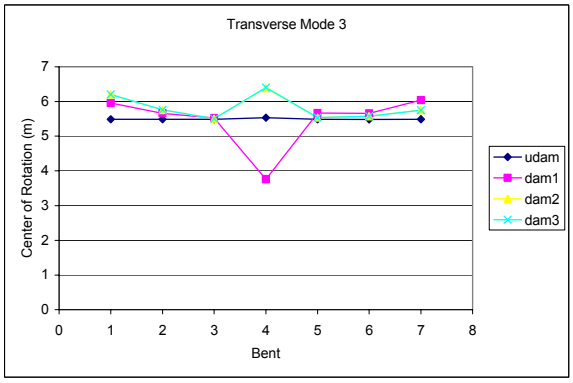

Plot C. Bent center of rotation transverse mode 3

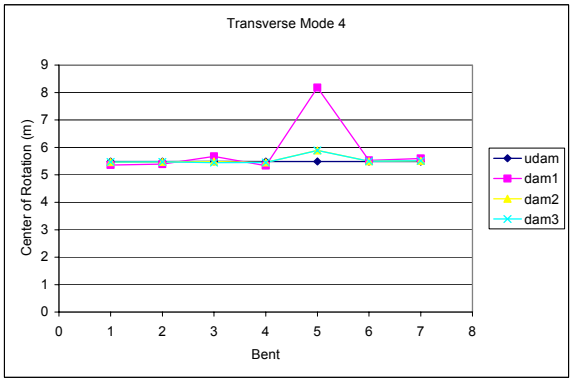

Plot D. Bent center of rotation transverse mode 4

FIGURE 3.9 Bent center of rotation plots.

CHAPTER 4

Finite Element Modeling of Six-Span Bridge at 500 South

Periodic inspection and testing of a structure is necessary to ensure its structural integrity and reliability. Visual inspection alone is not adequate to determine structural integrity. Internal damage and the damage in inaccessible areas are hard to detect in such investigations. Structural identification is a technique that may help to overcome these shortcomings. Developing the right analytical model of the structure plays a key role in ensuring that the model can be used in structural identification. Finite element modeling is the most commonly used tool in structural modeling. Finite element models usually have a high sensitivity to different structural parameters like stiffness, damping etc. Arriving at the correct values for these parameters is an important factor due to the model's high sensitivity to these values. Different kinds of iterative optimization algorithms have been developed to arrive at these values. This chapter discusses one such algorithm and shows the application of this algorithm to the finite element model of a six span bridge.

4.1 INTRODUCTION

Traditional condition assessment of bridges was done by visual inspection or by location dependent methods (Salawu and Williams, 1995). However such methods are highly dependent on the experience of the investigator and do not indicate the global structural integrity. In the recent years there has been a shift towards system identification and using dynamic characteristics as a means of assessing structural integrity. However its implementation in the field of civil engineering is a relatively new concept.

It is accepted that accurate prediction and simulation of dynamic behavior of structures requires analytical models that agree with the measured data (Cobb et. al, 1996). The accuracy of the obtained analytical model limits its usage as a system identification tool. The importance of the analytical model cannot be overemphasized in structural identification. The Utah State University Structural Engineering Division has recently conducted full scale forced vibration testing on a six span bridge. An eccentric mass shaker and an impact hammer were used to excite the bridge in the horizontal plane. Analysis of the collected data resulted in experimentally determined dynamic properties, namely frequencies of vibration, mode shapes and modal damping (Robinson et. al, 2000). This study was aimed at developing a model for the complete system identification of the bridge. A finite element model of the bridge was constructed to match the obtained natural frequencies as closely as possible to enable its use as an analytical tool for system identification of the structure. This paper describes the optimization technique used in arriving at the values of the parameters used in the finite element model.

4.2 BRIDGE DESCRIPTION

The structure tested was a free-standing, 109.73m (360.01 ft) six span, two-lane reinforced-concrete bridge (Figure 4.1). The deck was 18.29m (60.01 ft) by 7.39m (24.25 ft) and was made of 20cm (7.87 in) thick reinforced concrete slab. It was cast on I-shaped pre-tensioned concrete girders that were resting on neoprene bearing pads on the bent caps. These girders were connected to the bent-cap with dowel bars. The bents were made of 0.95m (3.12 ft) by 1.07m (3.51 ft) columns and a 0.95m (3.12 ft) by 1.68m (5.51 ft) bent-cap. The columns were supported by 3.35m (10.99 ft) by 3.35m (10.99 ft) by 1.07m (3.51 ft) reinforced concrete pile caps.

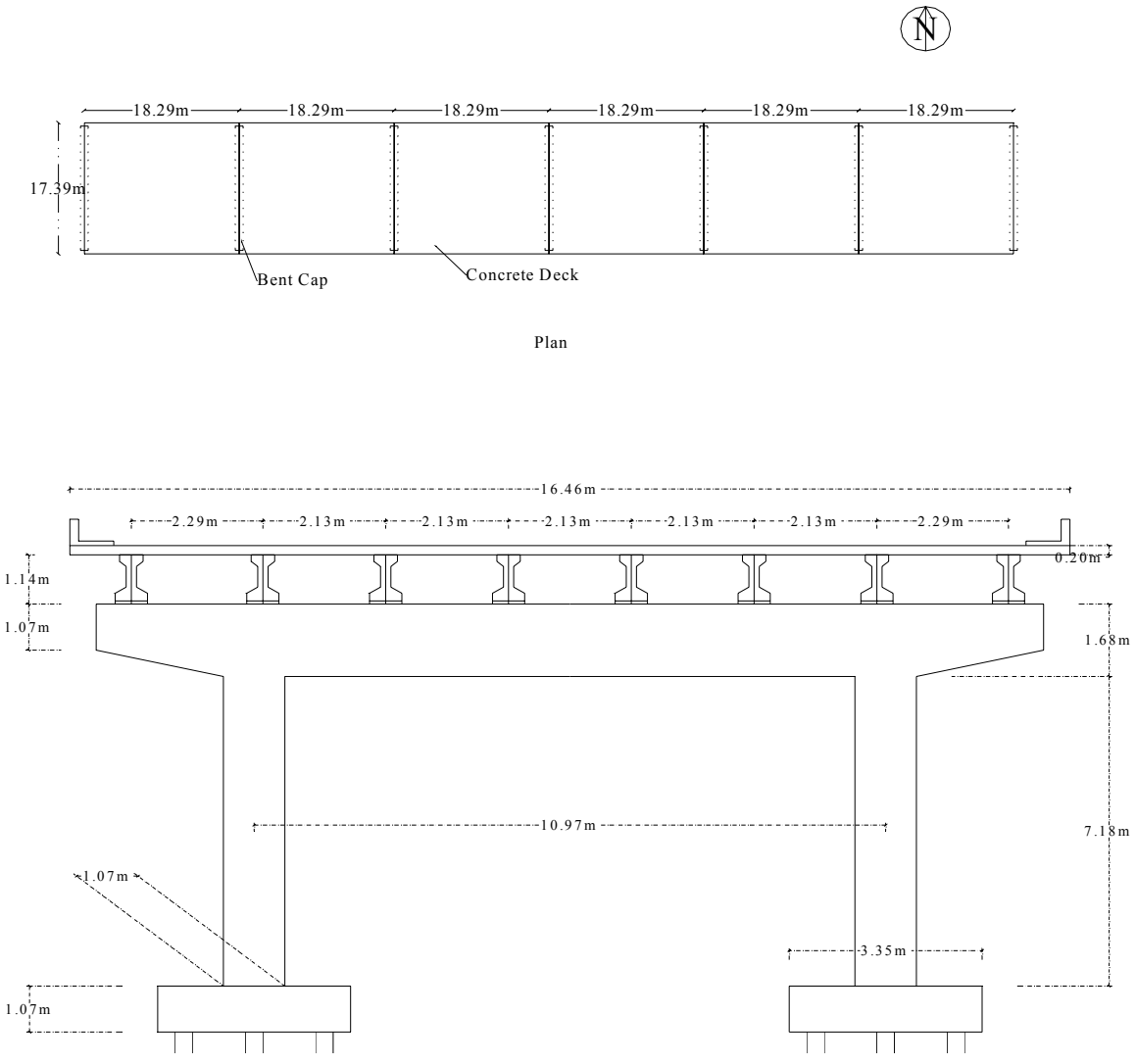

Figure 4.1 Plan and Elevation

4.3. MODELING

4.3.1 Finite Element Model Description

A finite element model was constructed using SAP2000 finite element analysis software. The columns, girders and the piles were modeled using frame elements. The piles were assumed to be fixed several feet below the ground level. This depth of fixity was later determined through the optimization procedure. The pile cap itself was modeled using rigid links from the base of the column to the piles. The concrete deck was modeled using thin shell elements. The shells and the girders were assumed to be rigidly connected. A typical detail of the expansion joint between the decks is shown in Figure 4.2. The neoprene pads between the girders and the bent-cap were modeled using springs in the horizontal plane in the x and y directions. The girders were assumed to be connected with the bent caps with dowel bars on one end and resting on the neoprene pads on the other. That is, one end of the girders was allowed to

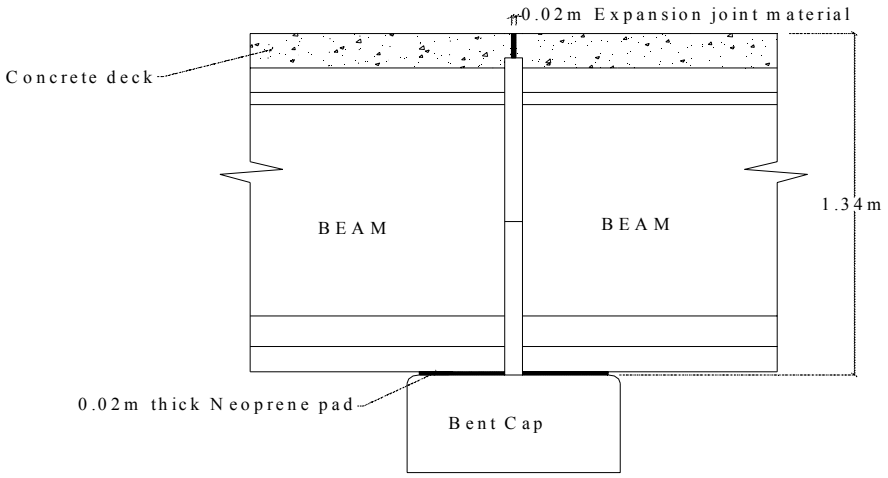

Figure 4.2 Joint Details

translate and rotate about the x and y directions, while the other end was pinned. The effect of the filler material and the expansion joint material were included in the model by adding weak springs in between the two decks at the joints. The finite element model of the bridge is shown in Figure 4.3.

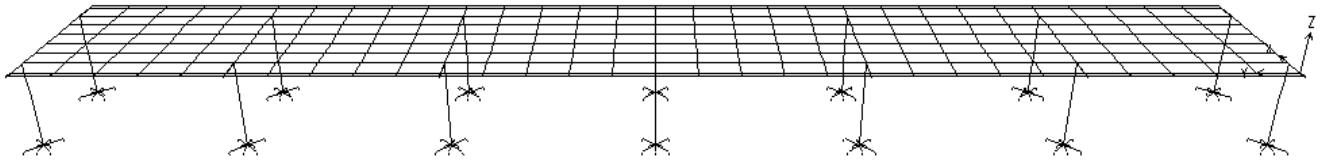

Figure 4.3. Finite element model – un-deformed geometry.

4.3.2 Parameters

The following are the parameters used in the optimization.

4.3.2.1 The depth to fixity of the piles

The pile groups at the bottom of the pile caps were assumed to fixed at a certain depth called the depth to fixity. This depth was expected to be less than the usually obtained values of the depth to fixity because the pile cap itself was under about 5 feet of soil cover.

4.3.2.2 The stiffness of the neoprene bearings

The neoprene bearings below the girders were modeled as springs and the effective stiffness of these springs was calculated as shown below. The force required to cause a deflection Δ, on the volume shown in Figure 4.4, is given by

$$F=(^{AG}/_{L})\,\Delta \qquad (4.1)$$

This value $^{AG}/_{L}$ was taken as the stiffness of the transverse springs that were used to model the bearings.

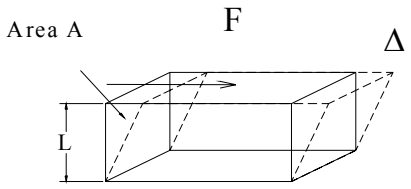

Figure 4.4 Transverse Stiffness

4.3.2.3 The modulus of elasticity of the concrete

It is generally agreed that the modulus of elasticity of concrete usually increases with age. The initial value of this parameter was therefore assumed accordingly.

4.3.3 Horizontal Mode Shapes

Analysis of the experimental data resulted in experimentally determined mode shapes in the horizontal plane and their natural frequencies. The first six natural frequencies were used in this optimization. The mode shapes were also replicated in the finite element model constructed. These mode shapes are shown below in Figures 4.5 to 4.10. Also indicated along with each mode shape is the period that corresponds to that particular mode shape.

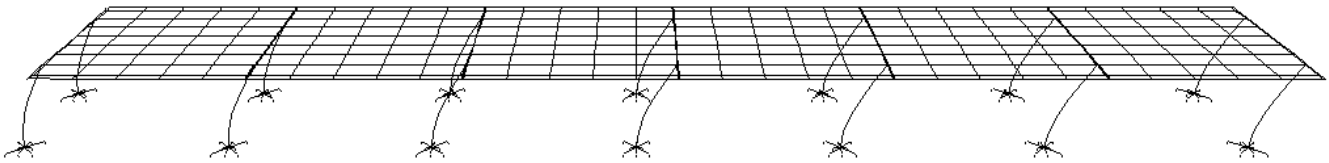

Figure 4.5: Mode 1, period = 0.8511s (longitudinal)

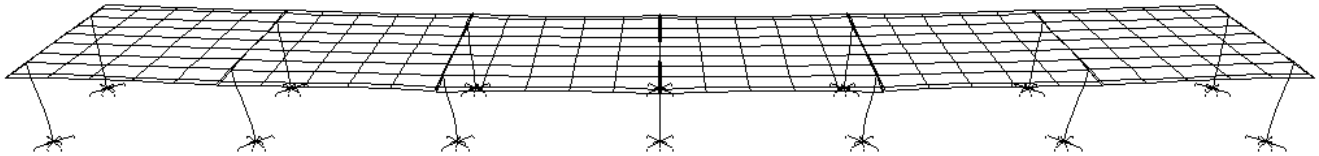

Figure 4.6: Mode 2, period = 0.4386s (transverse)

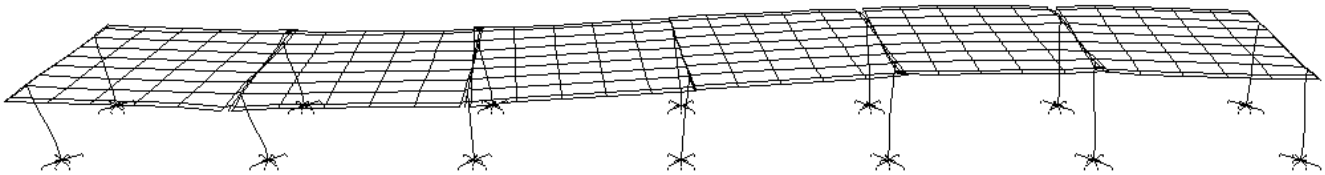

Figure 4.7: Mode 3, period = 0.3945s (transverse)

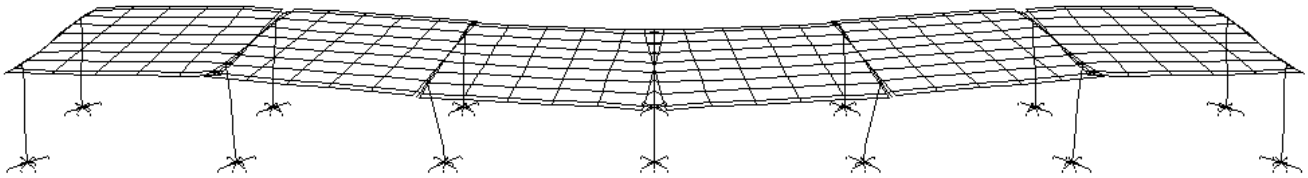

Figure 4.8: Mode 4, period = 0.3427s (transverse)

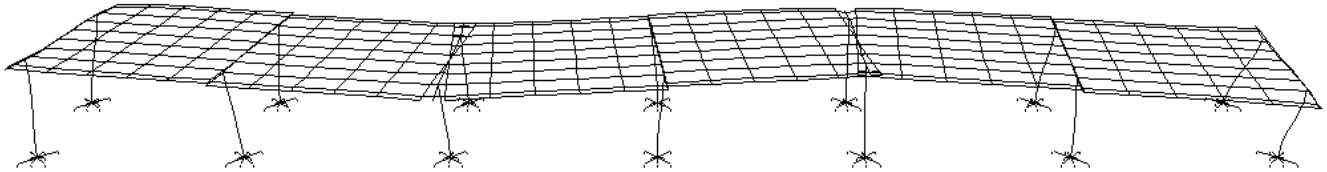

Figure 4.9: Mode 5, period = 0.2755s (transverse)

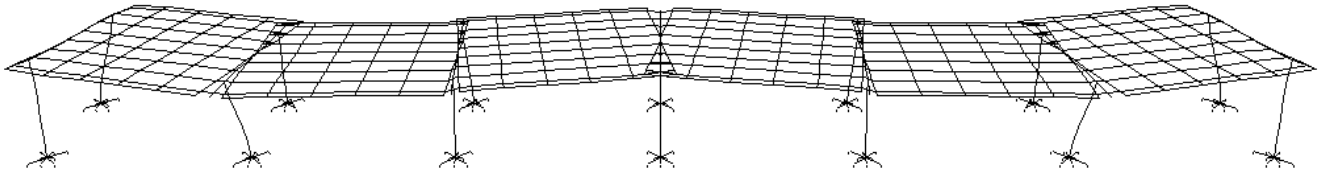

Figure 4.10: Mode 6, period = 0.2147s (transverse)

4.4. OPTIMIZATION

The aim of this optimization was to arrive at the values of the parameters (X_k), so as to match the natural frequencies of the bridge as closely as possible. The method proposed by Douglas and Reid (1982) was used for this optimization. The accuracy of the finite element model was estimated using the expression

$$E^2 = \sum_{i=1}^{m} \left(\frac{TF^i - TM^i}{TF^i} \right)^2 \tag{4.2}$$

in which m is the total number of modes considered for optimization (six in this case), where
TF^i is the observed period of the $i^{'th}$ mode of the bridge and
TM^i is the period of the $i^{'th}$ mode obtained from the finite element model.

4.4.1 Quasi-structural model

An ideal optimization algorithm would go through all the possible values of these structural parameters and try all the possible combinations. This however is an impractical approach. Instead, the computer model is used to create a quasi-structural model that is used to approximate the behavior of the finite element model. This quasi-structural model is defined by a second order polynomial as given below.

$$Q^i = C^i + \sum_{k=1}^{n} \left(X_k A_k^i + X_k^2 B_k^i \right) \tag{4.3}$$

in which n is the total number of parameters (three in this case). The (2n+1) unknown constants must be determined to complete the quasi-structural model. We first fix up the upper and lower bounds of these parameters to start the optimization procedures. It should be noted here that this procedure does not give results that lie within these bounds. These are only initial estimates chosen to start the procedure. To determine these constants we run the finite element model (2n+1) times. The model is first run with all the parameters at the base values. The model is then run 2n times varying each of the parameters to their lower and upper bounds and keeping all the other parameters at their base values. From each of these runs we then collect the periods (P^i) of the m modes that we are interested in. For each mode shape i this gives us a set of (2n+1) equations as shown below.

$$P_1^i = Q^i \left(X_1^b, X_2^b \ldots X_n^b \right)$$

$$
\begin{aligned}
P_2^i &= Q^i\left(X_1^l, X_2^b \ldots X_n^b\right) \\
P_3^i &= Q^i\left(X_1^u, X_2^b \ldots X_n^b\right) \\
P_4^i &= Q^i\left(X_1^b, X_2^l \ldots X_n^b\right) \\
P_5^i &= Q^i\left(X_1^b, X_2^u \ldots X_n^b\right) \\
&\vdots \\
P_{2n}^i &= Q^i\left(X_1^b, X_2^b \ldots X_n^l\right) \\
P_{2n+1}^i &= Q^i\left(X_1^b, X_2^b \ldots X_n^u\right)
\end{aligned}
\tag{4.4}
$$

These linear equations are then solved to arrive at the values of the (2n+1) constants for each mode shape. By solving the above equations for the constants we are forcing the quasi-structural model defined by Equation 4.3 to agree with the finite element model at the 3 values of each parameter – lower, upper and the base. The quasi-structural model so obtained is assumed to agree with the actual finite element model at all points for small domains. The validity of this assumption is further discussed in Douglas and Reid (1982).

4.4.2 The Newton-Raphson method

We now replace the finite element model by the quasi-structural model that we have formulated. As indicated earlier the optimization algorithm seeks to obtain the values of the parameters to minimize the error as calculated by Equation 4.2, i.e. we want to arrive at the values of X_k such that

$$
\frac{\partial E^2}{\partial X_k} = 0 \qquad\qquad 1 \le k \le n \tag{4.5}
$$

Substituting Equation 4.2 in Equation 4.5, we get

$$
\frac{\partial E^2}{\partial X_k} = \sum_{i=1}^{m} \frac{2\left(Q^i - TF^i\right)\left(A_k^i + 2X_k B_k^i\right)}{\left(TF^i\right)^2} \qquad\qquad 1 \le k \le n \tag{4.6}
$$

This gives us a set of n coupled equations of the variable X_k. The Newton-Raphson method for systems of equations was used to arrive at the roots of these equations (Khafaji and Tooley, 1986). In this method, we define functions $f_k(X_1, X_2 \ldots X_k \ldots X_m)$ as

$$
f_k\left(X_1, X_2 \ldots X_k \ldots X_n\right) = \frac{\partial E^2}{\partial X_k} \qquad\qquad 1 \le k \le n \tag{4.7}
$$

We have to arrive at the values of $(X_1, X_2 \ldots X_n)$ which make the function f_k go to zero. We now use Taylor series to evaluate these functions at $(X_1+h_1, X_2+h_2, \ldots X_n+h_n)$ by expanding the function about $(X_1, X_2 \ldots X_n)$. Thus we get the following equations

$$
f_k\left(\bar{X}_i\right) = f_k\left(X_i\right) + \sum_{j=1}^{n} h_j \frac{\partial f_k\left(X_i\right)}{\partial X_j} \qquad\qquad 1 \le k \le n \tag{4.8}
$$

It should be noted that we are using only a truncated Taylor expansion, i.e. we are including only the linear terms in this expansion. We now force these $f_k\left(\bar{X}_i\right)$'s to go be zero's and thus get an iterative formula for determining the values of these X_i's. These n equations finally reduce to the following form.

$$\begin{bmatrix} \frac{\partial f_1(X_i)}{\partial X_1} & \frac{\partial f_1(X_i)}{\partial X_2} & \cdots & \frac{\partial f_i(X_i)}{\partial X_n} \\ \frac{\partial f_2(X_i)}{\partial X_1} & \frac{\partial f_2(X_i)}{\partial X_2} & \cdots & \frac{\partial f_2(X_i)}{\partial X_n} \\ \vdots & \vdots & \ddots & \vdots \\ \frac{\partial f_n(X_i)}{\partial X_1} & \frac{\partial f_n(X_i)}{\partial X_2} & \cdots & \frac{\partial f_n(X_i)}{\partial X_n} \end{bmatrix} \begin{Bmatrix} h_1 \\ h_2 \\ \vdots \\ h_n \end{Bmatrix} = \begin{Bmatrix} f_1(X_i) \\ f_2(X_i) \\ \vdots \\ f_n(X_i) \end{Bmatrix} \tag{4.9}$$

i.e. $[J]\{h\} = \{f\}$ and $\left\{\bar{X}\right\} = \{X\} - [J]^{-1}\{f\}$

This gives us the iteration formula

$$\{X\}_{k+1} = \{X\}_k - [J]_k^{-1}\{f\}_k \tag{4.10}$$

When this formula is applied to the quasi-structural model we get

$$J(k,j) = \sum_{i=1}^{m} \left\{\left(A_j^i + 2X_j B_j^i\right)\left(A_k^i + 2X_k B_k^i\right)\right\} \qquad \text{if } k \neq j$$

$$J(k,j) = \sum_{i=1}^{m} \left\{\left(A_k^i + 2X_k B_k^i\right)^2 + 2\left(Q_i - TF_i\right)B_k^i\right\} \qquad \text{if } k = j \tag{4.11}$$

The base, the lower and the upper bound values are initially assumed. The quasi-structural model is then formulated from these values. The obtained constants and the base values are then substituted in Equation 4.10. This gives us the next set of base parameters to go on. This iteration process is then continued till the parameter values stabilize. As mentioned before, it should be noted that this algorithm does not guarantee results within the assumed lower and upper bounds. The obtained optimized parameter values are then used in the finite element model only if they are feasible. If the results obtained are not accurate enough, then a new search domain is defined by using these optimized values as the base values. This, as a result, narrows down the search space. Engineering judgment should be used when deciding whether the obtained values are feasible. If unacceptable values are obtained it is usually an indication that the chosen base values are wrong or that the finite element model cannot be described adequately by the chosen parameters. This process is continued until a desired accuracy is obtained. The flowchart for this procedure is given below in Figure 4.11.

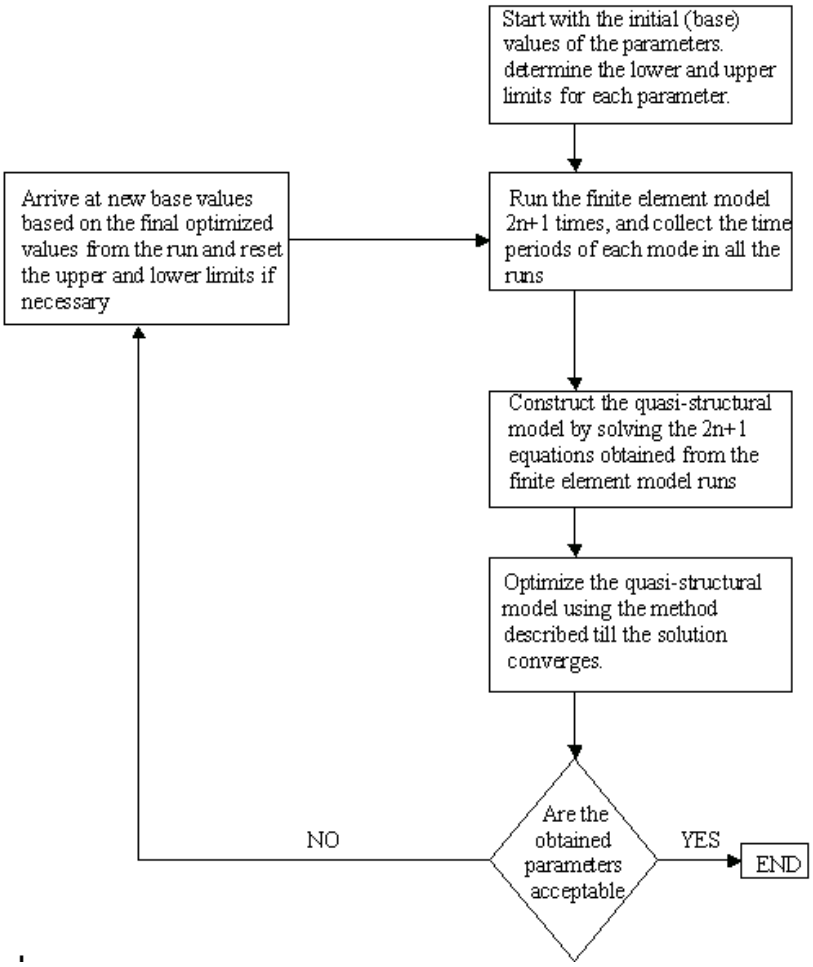

Figure 4.11 Flowchart

4.5. RESULTS

The three parameters described earlier i.e. 1) the depth to fixity of the piles, 2) the stiffness of the neoprene pads and 3) the modulus of elasticity of the concrete were all used in the optimization. The optimization program was written using C++ and the finite element model was constructed and run in SAP2000. The results of the optimization runs are presented below. The optimization program was run three times starting with a set of base values and then using progressively refined base values in the subsequent runs.

Table 4.1: Run Number 1

Parameters	X_1 N/mm	X_2 m	X_3 N/mm^2	Error
Run #1	Neoprene pad stiffness	Depth to fixity of the pile group	Modulus of elasticity of concrete	Error as calculated by the q-s model (eqn.4.2)
Base values	10947	0.3048	22743	

Lower bound	7298	3.048e-3	21546	
Upper bound	14596	0.6096	23940	
Optimized values	20295.3	0.4806	29533.05	0.0758984

The optimized values obtained in the run that are shown above (Table 4.1) were then modified and used in the next run (Table 4.2). The optimization was done using the fps system, and so even minor modifications appear as large numbers due to conversions. It can be seen that the total error as calculated by the optimization program (Equation 4.2) decreases in the following run.

Table 4.2: Run Number 2

Parameter	X_1 N/mm	X_2 m	X_3 N/mm^2	Error
Run #2	Neoprene pad stiffness	Depth to fixity of the pile group	Modulus of elasticity of concrete	Error as calculated by the q-s model (eqn.4.2)
Base values	20434.4	0.4877	28728	
Lower bound	17515.2	0.3048	23940	
Upper bound	23353.6	0.9144	33516	
Optimized values	42126.7	0.5318	24971	0.0439997

The values obtained in this run were again modified and used in the next run as shown below.

Table 4.3: Run Number 3

Parameter	X_1 N/mm	X_2 m	X_3 N/mm^2	Error
Run #3	Neoprene pad stiffness	Depth to fixity of the pile group	Modulus of elasticity of concrete	Error as calculated by the q-s model (eqn.4.2)
Base values	36490	0.5334	24897.6	
Lower bound	21894	0.3048	23940	
Upper bound	43788	0.9144	26334	
Optimized values	35699	0.5706	24620	0.0331718

It can be seen from the above tables that in the third run the optimization has almost reached a stable state. The process can be stopped here or it can be taken further if more accuracy is desired. The final values that were obtained after the third run were used in the finite element model and the results are shown below (Table 4.4) along with the results obtained by using the optimized values from the other two runs. The errors, as calculated by Equation 4.2 are also presented.

Table 4.4: Actual model comparison

	Mode 1 – period (s)	Mode 2- period (s)	Mode 3- period(s)	Mode 4- period(s)	Mode 5- period(s)	Mode 6- period(s)	Error
Experimentally determined	0.8511	0.4386	0.3945	0.3427	0.2755	0.2147	
Run #1 Optimized	0.7281	0.3232	0.3620	0.3275	0.2888	0.2502	0.1285
Run #2 Optimized	0.7777	0.3938	0.3671	0.3269	0.2840	0.2387	0.0383
Run #3 Optimized	0.7848	0.3992	0.3730	0.3329	0.2901	0.2455	0.0413
% Error using the results from Run #2	8.6	10.2	6.9	4.6	-3.1	11.2	

A few points should be noted in the above table. Although the quasi-structural model predicted a closer agreement in between the optimized model and the actual field observations, the finite element model does not reflect this. This is due to the differences between the finite element model and the quasi-structural model (which is a mathematical representation of the finite element model's behavior). The major difference between the optimized values of the second and the third runs lies in the value of the transverse stiffness of the neoprene pads. The other two quantities, the depth to fixity of the piles and the modulus of elasticity of concrete have stabilized. The final optimized values can be taken as those obtained after the second run or, the model can be run a few more times varying the first parameter in between the two values, without having much variation in the other two parameters.

4.6 CONCLUSIONS

It can be seen from the above example that this method of optimization yields results that are acceptable and converge fairly quickly to the result. The figures obtained, as shown in Table 4.4 are fairly accurate and the maximum error is only eleven percent. This, however, can be decreased if more runs are performed. The following points (drawbacks) should be noted when this method of optimization is used in practice.

The results obtained in the intermediate runs need not lie with the upper and lower bounds set before the optimization is run.

The results may be erroneous values when the initial base values are not properly estimated. However this is usually caught easily because it would yield results that are ridiculously high or low. This is not a problem because the modeler usually has a rough estimate of what the parameter values should be.
By increasing the number of parameters, the finite element model can be made to better match the obtained experimental results. This would however lead to an increase in the computational time as the finite element model would have to be run 2n+1 times where n is the number of parameters to be optimized.

This process cannot be completely automated and the user should watch the optimized values and reset them whenever necessary using judgment.

CHAPTER 5

Impact testing at bents and at six-span bridge

Non-destructive detection of damage to structures has developed over the last few decades. This chapter focuses on various facets of modal testing performed on various highway structures along the I-15 corridor in Salt Lake City, Utah. Several conclusions pertaining to modal testing procedures, analysis, and results were obtained during this study.

Two methods were used to excite the I-15 bridge structures: an eccentric rotating mass shaker and an impulse force vibration. Nine vibration tests on three isolated bents were performed. Sixteen addition vibration tests were executed on a six span bridge structure. Both of these series of test were rendered over various controlled damage states.

Three states were measured for each of the three bent caps and four for the six-span structure. The first state was the original condition of the structures before any purposeful damage was done. The other states were chosen to represent the types of damage that might be created by an earthquake and were inflicted to both the columns and foundations. The damage states are illustrated in Figure 5.1.

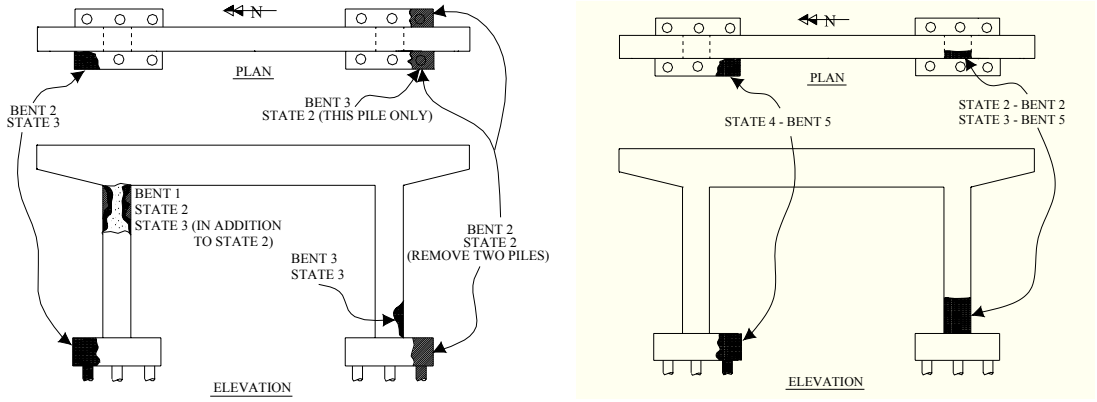

Figure 5.1. Illustration of Damage States for the Bents (left) and the Six-Span Structure (right).

Various structural and modal parameters were obtained from the above mentioned experiments. These results were investigated for various interesting phenomena. These results and phenomena are discussed in the following list:

Effects of Pads and Expansion Joints
Independent Modes of Slabs at High Frequencies
Bent Damage States
Data Quality Between Bents
Comparison of Impact and Eccentric Mass Vibration Testing

In addition to these phenomena, this chapter reviews various analytical techniques utilized to obtain desirable results from modal testing. The first of these are methods of using macros to process the data. Additionally, curve fitting methods for modal peaks and calibration curves were used. Furthermore, a calibration procedure to produce reliable results from low-frequency geophone response will be discussed.

5.1 ANALYSIS PROCEDURES

In general two methods were used to process and prepare the impact experimental data for modal analysis. The bent data was processed on site and the six-span data was processed after the fieldwork was completed. Both were used to obtain a relationship between displacement per unit force and phase response verses frequency, and these in turn were utilized to obtain the modal information. Modal parameters include the natural frequency, damping, phase, and mode shapes.

Due to the noisiness of the data and the inherent difficulty of determining the modal parameters of each mode, a curve fitting macro was produced. The equation used to fit the modal peaks to determine the natural frequency (f_n), damping (D) and pseudostatic stiffness (g) is given as:

$$f_n = g\frac{\sqrt{1+(2D)^2}}{\sqrt{(2D)^2}} \tag{5.1}$$

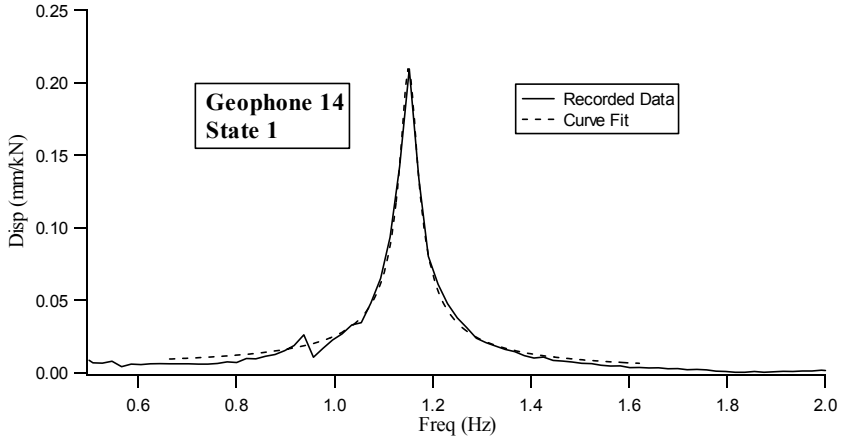

Figure 5.2. Modal Peak and Fit Curve

The damped and undamped natural frequencies for impact testing as well as the phase at resonance were also produced by the macro. The phase and magnitude of displacement at each modal frequency were utilized to create the mode shapes for the structures. An example of a modal peak fit utilizing the macro is presented in Figure 5.2.

Calibration curves were created for the accelerometers and geophones using information provided by the manufacturer. This calibration is critical to take advantage of the higher output of the geophones at low frequencies. Laboratory methods of calibrating velocity transducers to determine the coefficients that describe their behavior were produced as part of this study. These laboratory results were compared with those provided by the manufacturer.

5.2 RESULTS

5.2.1 Geophone Calibration

Characterization parameters produced in the laboratory were compared with those provided by the geophone manufacturer. They generally agreed within a few percent with select geophones deviating as much as 43 percent from select manufacturer provided parameters. These results indicate that the geophone calibration parameters supplied by the manufacturer may differ from their actual response. Often, the manufacturer provides non-individualistic parameters or no parameters at all. For these reasons, it is important that geophones are carefully calibrated at low frequencies to produce reliable data in this range.

5.2.2 Bent Modal Data

Once the bent data from the impact testing was collected and analyzed, the modal data was obtained. The information for the first mode of each bent is given below in Table 5.1.

Table 5.1. First Mode Data for Bent

Mode 1x	Natural Frequency (Hz)			Damping (%)		
	State 1	State 2	State 3	State 1	State 2	State 3
Bent 1	3.949	3.970	3.931	1.99	1.66	1.86
Bent 2	3.844	3.624	3.552	1.36	1.20	1.95
Bent 3	4.148	4.044	3.795	1.96	2.05	1.63

The mode shapes for the first modes of the three bents are shown in Figure 5.3.

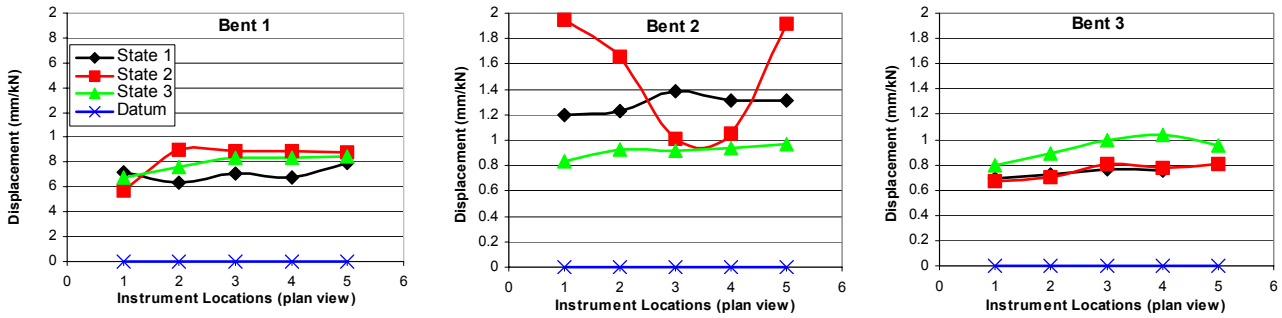

Figure 5.3. First Mode Shape of the Bents

5.2.3 Six-Span Structure Modal Data

The modal data for the first modes were produced from the collected impact test data. The first three modes, one longitudinal (1y) and two transverse (1x and 2x), produced from an impact of 45 degrees on the deck slab are tabulated in Table 5.2.

Table 5.2. Modal Data for Modes 1y, 1x and 2x for the Six-Span Structure.

6-Span 45□ Imp.	Natural Frequency (Hz)				Damping (%)			
	State 1	State 2	State 3	State 4	State 1	State 2	State 3	State 4
Mode 1y	1.153	1.121	1.112	1.142	1.53	1.57	1.27	1.75
Mode 1x	2.324	2.321	2.316	2.315	3.20	3.52	3.22	3.10
Mode 2x	2.545	2.493	2.491	2.550	3.08	3.92	3.46	3.56

The mode shapes for the first three modes are shown in Figure 5.4.

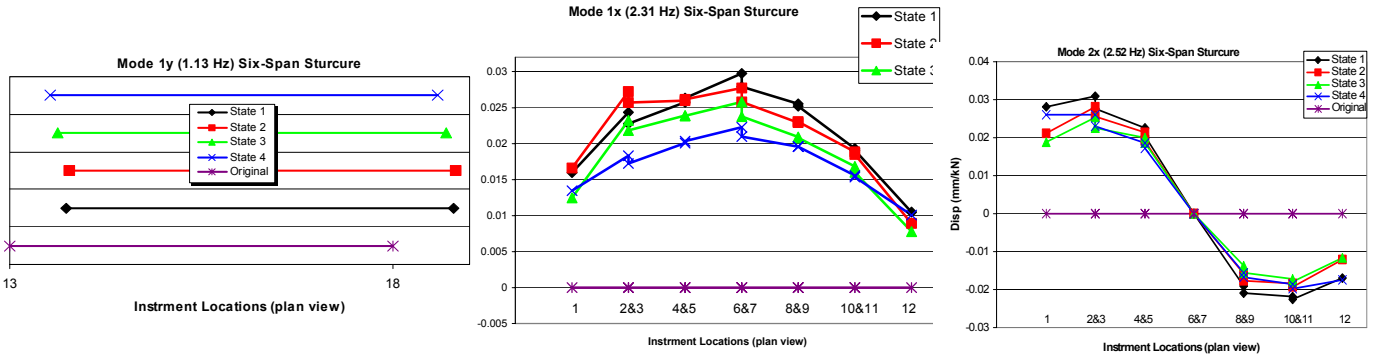

Figure 5.4. First Three Mode Shapes of Six-Span Structure

5.2.4 Effects of Pads and Expansion Joints

To examine the effects of the pads between the bent caps and the bridge deck and the expansion joints between the slabs of the deck, the response of three horizontal geophones were compared. Two geophones were positioned just east and just west on either side of an expansion joint, directly above a bent upon which the third geophone rested. The hammer impact was effected on this same bent cap, as well as on the east slab above the bent cap and on the west slab in the same general location.

Little difference was noted in the three geophone's responses to the different impact locations at frequencies up to approximately seven to eight Hertz. This indicates that the entire structure is moving in phase and the joints and pads have little effect on the response.

Next, the frequency span from 8 to 60 Hertz was examined. At the higher frequencies, the geophone situated on the section of the structure that is impacted moves in phase with the impact and the other two

are cycling in and out of phase. At these higher frequencies, we also see a difference in the amplitudes. The amplitudes of the impacted portion are much higher than that of the un-impacted. This is consistent for all three impact locations. At even higher frequencies, we see a more exaggerated effect of these phenomena.

It appears that the structure stops moving as a rigid body and its component parts begin to move independently around seven to eight Hertz. This seems to be where the joints and pads start controlling the motion. Definitely above 60 Hertz, a large portion of the energy is being adsorbed by the pads and joints.

5.3 CONCLUSIONS

5.3.1 Independent Modes of Slabs at High Frequencies

Another important point is that at higher frequencies, the mode shapes between the slabs do not coincide. The modes match up well at the low frequencies. Once the natural frequencies exceed about seven Hertz, the modal peaks no longer match up for all channels. At the much higher frequencies, it appears that each slab has its own modal shapes that do not correspond to a global mode. This phenomena also indicates that much of the energy is being absorbed by the joints and pads at these higher frequencies as was noted in the previous section.

5.3.2 Bent Damage States

The modal shapes produced by the bent impact test data were examined to attempt to locate the position where damage occurred. The results were mixed. The most consistent indicator of damage bents was the decrease in the natural frequencies. Damage location was not clear from the majority of the results. One mode on the third bent did indicate damage and general location very well.

5.3.3 Data Quality Between Bents

For the impact testing, data quality was directly proportional to the amount of force imparted to the structure. This seemed to be a larger influence on the quality of the data than the number of averages. For first two damage states on one of the bents, the impacts were of minimal force and the third time, efforts were made to maximize the force without going outside the linear range of the instrument. The third damage state indicated significantly higher quality data at low frequencies. The higher frequency data was not effected as much by the differences in effort.

5.3.4 Comparison of Impact and Eccentric Mass Vibration Testing

This section will present a comparison of the two types of sources utilized to excite the bent structures: a monochromatic source and a broadband energy source. The rotating eccentric-mass shaker provides

high-quality data over a limited frequency range, while the impulsive source produces lesser quality data over a much wider range of frequencies. An example of the quality of data produced at frequencies from zero to twenty Hertz by the impact testing (left figure) and shaker (right figure) can be seen in Figure 5.5.

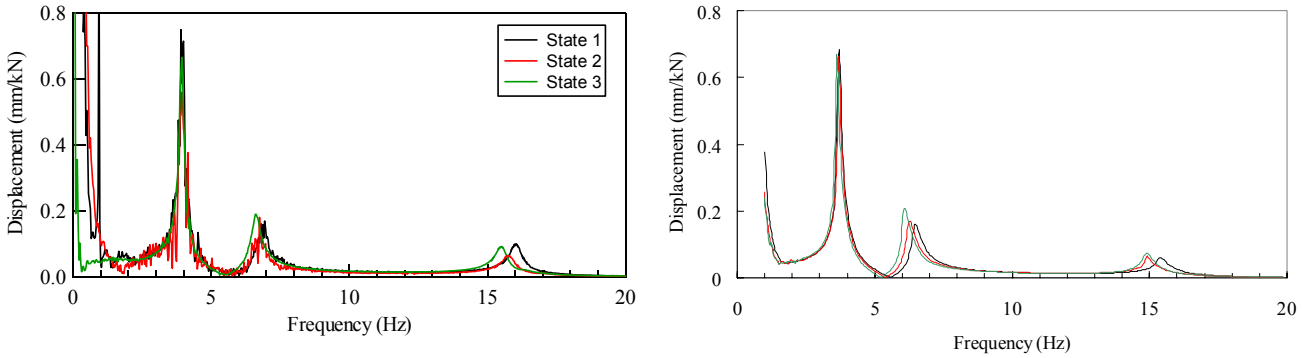

Figure 5.5. Data Quality Comparison Example.

The impulsive source also requires significantly less testing time and simpler data analysis than the rotating eccentric-mass shaker. The majority of the modal parameters produced by both sources correspond well. However, the natural frequencies produce by the shaker are generally 0.4 to 1.2 Hertz higher than those produced by the impact excitation. A comparison of damped and undamped natural frequencies for both sources did not fully account for the differences. Non-linear response of the structures due to the larger displacements produced by the shaker is a plausible cause of this discrepancy.

CHAPTER 6

Three-span bridge at 300 North

Forced vibration testing has been used for condition assessment of bridges in the past. To be considered a valid method of condition assessment, forced vibration testing must be reproducible. Nine tests were performed on a three span bridge on Interstate 15 using forced vibration. Velocity transducers were used to acquire the response of the bridge. Three test parameters were altered for four of the tests. These parameters were temperature, the amount of forcing and the direction of forcing. Forced vibration testing was repeated and analysis was performed to determine the variability in both testing and analysis. Dynamic properties investigated include natural frequencies, mode shapes, and modal damping.

6.1 INTRODUCTION

The need for a consistent method of condition assessment is crucial to the state of our nation's transportation infrastructures. Currently, visual inspection is the most widely used method for assessing structural integrity. Various problems arise from visual inspection. The experience of the responsible parties inevitably varies, thus making it difficult to maintain a level consistency from one inspection to another.

With the rapid progress of technology over the past couple of decades, dynamic testing of structures has become more feasible. One method of dynamic testing is forced vibration. Forced vibration testing can be used to determine the dynamic characteristics of bridges. Vibration testing is based in the concept that dynamic response relates to changes in mass, stiffness, or damping of a structure. Changes in these characteristics affect modal properties such as natural frequencies, mode shapes, and modal damping. Previous research by Tsai and Yang (1988) has shown that the magnitude of change in parameters like the mass and stiffness matrices are proportional to the amount of deterioration experienced by a structure. Monitoring these modal properties for changes becomes the focus of vibration testing. Once a baseline is established for a particular structure, further tests are performed as required and analyzed in comparison to the baseline.

This methodology is based on the assumption the modal properties derived from the testing are unique and the results will be the same each time the test is performed as long as the conditions have not changed. A full-scale three span bridge was tested multiple times using forced vibration. The results from one series of tests are presented in this chapter.

6.2 EXPERIMENTAL SETUP

6.2.1 Bridge Description

The three span bridge tested was a southbound overpass structure of Interstate 15 in Salt Lake City, Utah. This bridge was in service just prior to demolition. The bridge consisted of three simple spans of 14.4 m (47.25 ft), 21.0 m (69 ft), and 14.4 m (47.25 ft), with a width of 18.3 m (60 ft) and skew of 1.5°, as depicted in Figure 6.1. The deck is made up of two parts, 102 mm (4 in) of asphalt over a 178 mm (7 in) concrete deck. There are 8 steel girders supporting each span, resting on steel bearing bars. The reinforced concrete bents and columns are 1220 mm x 915 mm (4 ft x 3 ft) and 915 mm x 915 mm (3 ft x 3 ft), respectively. For ease the spans and bents have been numbered from south to north.

6.2.2 Equipment and Instrumentation

An eccentric mass shaker provided the forcing to excite the bridge. The machine is comprised of two masses attached to spindles with a center-to-center distance of about one meter. This shake can only produce forcing in a horizontal plane. The masses can be adjusted so that as they rotate in opposite directions they can be oriented to produce forcing along a linear line. By vectorially summing the radial forces of both masses, the machine produces a sine function in the horizontal plane. The masses can also be set to offer various eccentricities to control the amount of forcing generated.

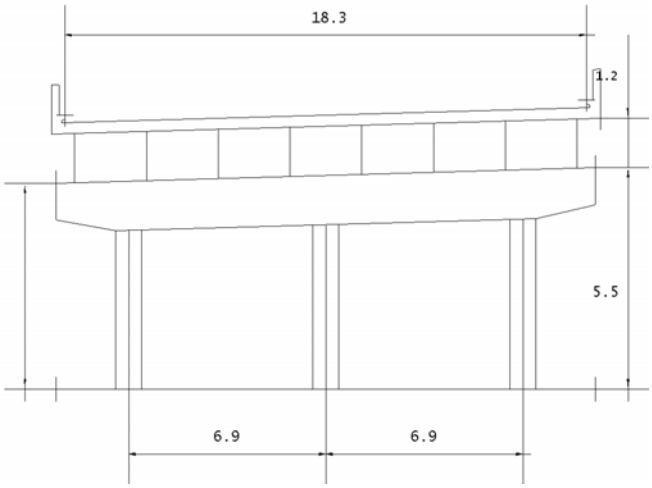

Figure 6.1. Cross section of the bridge.

The instruments used to capture the response of the bridge were L-4C 1.0 Hz Geophones. These seismometers were calibrated to allow the conversion of the voltage output to a velocity. Nineteen seismometers to measure horizontal velocities were used to instrument the deck of the bridge. Twelve more seismometers were mounted on the two bents. Four of these measured vertical velocities.

National Instruments software installed on a personal computer was used to control the National Instruments data acquisition system. The velocity transducers and the eccentric mass shaker were

plugged into the acquisition system. Each cable was numbered and the seismometer-cable combination was tracked to enable the combination to remain the same throughout all tests.

6.3 TESTING

A module in the software was designed to initiate the machine rotating. After the bridge arrived at a steady state condition for a given frequency, the module commenced acquiring the data from the velocity transducers and shaker. A sinusoidal sweep from 0.5 to 16 Hz, stepped at .02 increments, was used to induce the response of the bridge. Data was recorded for approximately 20 seconds at a sampling rate of 500 samples per second for increments between 0.5 to 9 Hz and 13 seconds at a sampling rate of 640 samples per second for the 9 to 16 Hz range. The module saved the raw data to a file on the personal computer. Files were saved in 2 Hz increments. These files were later transferred to compact discs because of their size.

6.4 ANALYSIS

A demodulation program was used to filter out the noise from the response signal. Similar to how an AM radio signal is received and processed, the response signal from the seismometer had to be separated from the noise. In AM radio the signal is mixed with a carrier wave and then separated from the carrier wave upon reception. In this case the response signal is the carrier wave and the noise is mixed in with it.

In order to perform this filter the operating frequency must be known. As discussed in the previous section, data from the machine was taken and recorded with the response data. An encoder on the machine sent a voltage spike each time the forcing occurred in the desired direction. These spikes are used to calculate the frequency of the machine. At steady state the frequency of the instruments was the same as the operating frequency of the shaker. The following equation describes the signal created by a seismometer.

$$g(t) = f(t) \cos(\omega_0 - \varphi(t)) + n(t) \tag{6.1}$$

where $g(t)$ = output voltage signal
$f(t)$ = amplitude of the signal
ω_0 = operating frequency of the shaker
$\varphi(t)$ = absolute phase lag of the seismometer
$n(t)$ = noise

The signal amplitude can be expressed as

$$f(t) \cos(\omega_0 - \varphi(t)) = a(t) \cos\omega_0 t + b(t) \sin\omega_0 t \tag{6.2}$$

where *a* and *b* are constants are of the complex form

$$a(t) + ib(t) \tag{6.3}$$

The amplitude f(t) can be calculated by taking the square root of the sum of the squares of a(t) and b(t) (Bay,1997).

Once the voltage amplitude was obtained through demodulation, it was converted to a velocity output. This was done by using the calibration curve for each seismometer. From velocity, displacement was calculated. The displacement was normalized because forcing is a function of the operating frequency such that it is measured in displacement per unit force (mm/KN). Equation 6.4 describes the normalization:

$$\frac{\text{displacement}}{\text{force}} = \frac{V}{2\pi C_f f} = \frac{\text{mm}}{\text{KN}} \tag{6.4}$$

where V = voltage output of seismometer
C_f = calibration curve for an individual seismometer
$f = 2.0958\omega_0^2$, the force produced by the shaker
ω_0 = operating frequency of the shaker

Using this format the raw data was transformed for each instrument into a response in terms of displacement per unit force and relative phase lag for the corresponding frequency.

6.5 RESULTS

With the data in this format, displacement response spectrums were created by plotting the displacement versus frequency. This was done for each of the instruments to determine the natural frequencies. Figure 6.2 is an example a displacement response spectrum.

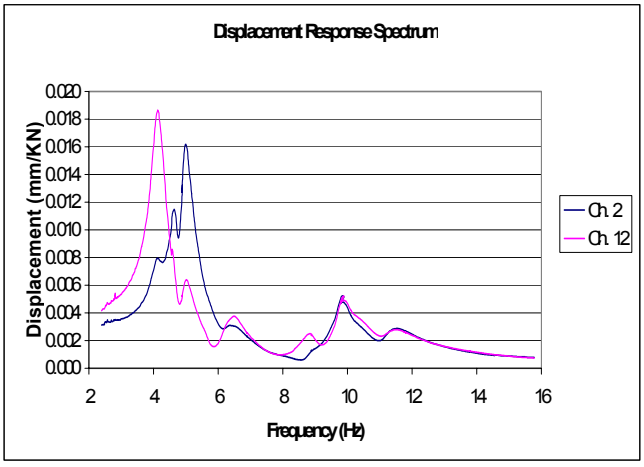

Figure 6.2. Displacement Response Spectrum for seismometers 2 and 12.

A natural frequency is defined as the frequency where maximum amplitude of displacement is achieved. To aid in accurately selecting the natural frequency, a cubic spline fit was used to create an additional 10 points between two original data points. By adding these points, the precision of the natural frequencies can be taken in terms of thousandths of a Hertz versus hundredths of a Hertz.

The natural frequency for each mode was determined by selecting the three seismometers that exhibited the largest displacement and by taking the average of the three. For the purpose of this discussion only, the first three modes will be examined. Table 6.1 contains the results of the natural frequencies for one set of tests.

Modal damping was found by using the half power-power bandwidth method. This method uses the relationship between frequency and displacement. The maximum displacement of a mode is divided by square root of 2. Two frequencies correspond to the factored displacement. Equation 6.5 uses the two frequencies to calculate the modal damping.

$$D \cdot \frac{(f_2 - f_1)}{(f_2 + f_1)} \tag{6.5}$$

where D represents the damping ratio

f_2 = largest corresponding frequency to the maximum displacement divided by $\sqrt{2}$

f_1 = smallest corresponding frequency to the maximum displacement divided by $\sqrt{2}$

Table 6.1. Comparison of natural frequencies for one set of tests.

		Ch.	Freq.	Ave. Freq.
Mode 1	Test 1	12	4.134	4.139
		14	4.140	
		19	4.144	
	Test 2	12	4.132	4.145
		14	4.144	
		19	4.160	
Mode 2	Test 1	2	4.620	4.623
		13	4.624	
		18	4.626	
	Test 2	2	4.636	4.646
		13	4.648	
		18	4.654	
Mode 3	Test 1	2	4.908	4.908
		15	4.912	
		22	4.904	
	Test 2	2	4.990	4.993
		15	5.006	
		22	4.984	

The half power-power bandwidth method could only be used on the first mode. The same seismometers used to find the natural frequencies were used to calculate the damping ratio for each test. Table 6.2 lists the average damping ratios.

Table 6.2. Average damping ratios.

Average Damping Ratio for Mode 1	
Test 1	5.18%
Test 2	5.80%

Using the nodal displacements that correspond with the natural frequencies previously found, the mode shapes were defined for each test. The direction of the displacement was determined by the relative phase angle for each seismometer. Phase angles near +90° represent displacement in the positive direction or North for longitudinal oriented instruments and East for transverse oriented instruments. Angles near -90° represent displacement in the South or West direction for longitudinal or transverse orientations, respectively.

In determining the transverse mode shape of mode 1, only seismometers oriented transverse on the bridge were used. Likewise, only longitudinally oriented seismometers were used for the longitudinal mode shapes. To simplify the mode shapes, the deck of each span is assumed to be rigid and the displacements are taken at the center of each span. The following three plots are the mode shapes for the three modes.

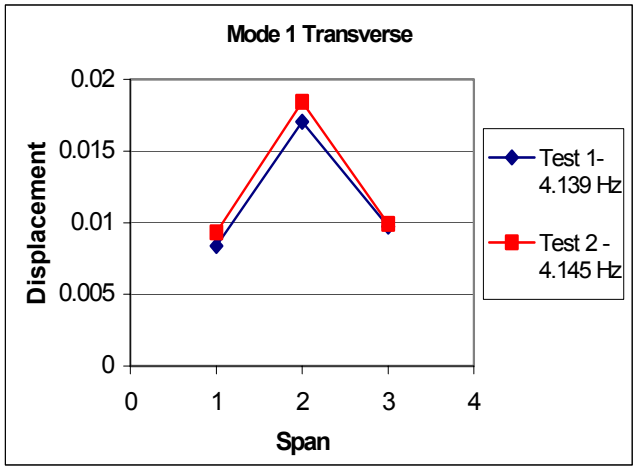

Figure 6.3. Transverse mode shape from mode 1.

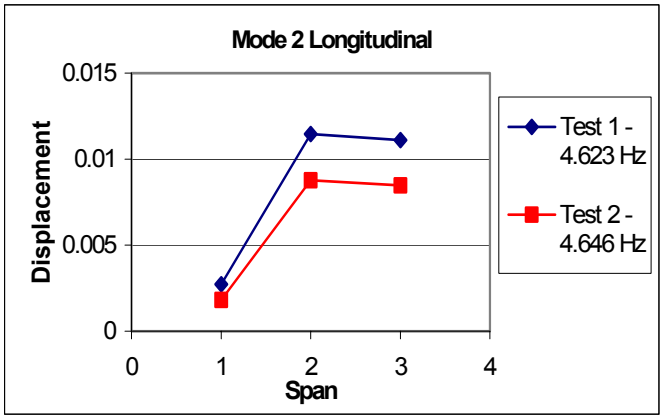

Figure 6.4. Longitudinal mode shape from mode 2.

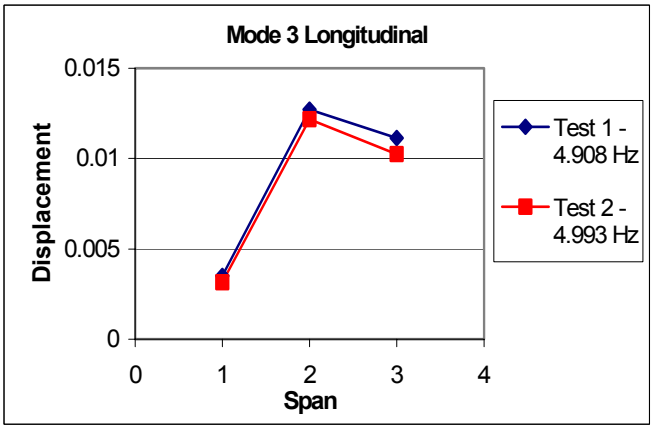

Figure 6.5. Longitudinal mode shape from mode 3.

6.6 CONCLUSIONS

Modal damping for both tests was between 5% and 6%. From Test 1 to Test 2 it experienced a 12% increase. Salawu and Williams (1995) noted that the inconsistency in modal damping excludes itself from being used as a means of integrity assessment. The natural frequencies, on the other hand, experienced minor increases. Mode 1 saw a 0.1% increase; mode 2, a 0.5% increase; and mode 3 experiencing the largest increase at 1.7%. These numbers affirm previous findings by Robinson et al. (2000) and Muhammad et al. (1999) that natural frequencies are consistent enough to use for damage detection. However, natural frequencies are global parameters and offer little in pinpointing localized damage. With the mode shapes exhibiting only a small change similar to that of the natural frequencies, they could be used for condition assessment. Modes shapes typically offer a better picture of any local affects than do natural frequencies.

In conclusion, forced vibration testing using an eccentric mass shaker is a valid method for determining condition assessment. It is a practical method for performing routine and event driven inspections.

CHAPTER 7

Acknowledgements

The authors wish to gratefully acknowledge the Utah Department of Transportation (UDOT) and the Federal Highway Administration (FHWA) for the funding that made this research possible. In addition, the authors acknowledge Wasatch Constructors and the Penhall Company for their support and cooperation in the completion of this project. Our appreciation also goes out to Mr. Stephen Bott, Mr. Bryant Nielson, Mr. Kenneth Jewkes, and Dr. Ikhsan Muhammad for their countless hours in the field and lab.

CHAPTER 8

References

Aktan, A. E., Farhey, D. N., Helmicki, A. J., Brown, D. L., Hunt, V. J., Lee, K. L., Levi, A. (1997). *Structural identification for condition assessment: experimental arts.* J. Struct. Engrg., ASCE, 123(12), 1674-1684.

Al-Khafaji, Amir Wadi and John R. Tooley (1986) "Numerical methods in engineering practice" CBS college publishing. ISBN 0-03-001757-2.

Bay, J. A. (1997). *Development of a rolling dynamic deflectometer for continuous deflection testing of pavements.* Ph.D. Dissertation, University of Texas at Austin.

Cobb, Richard G., Robert A. Canfield, and Brad S. Liebst (1996). "Finite element model tuning using automated structural optimization system software". AIAA Journal.Vol. 34, No. 2, 392-399

CSI. *SAP2000 Analysis Reference Volume 1. Version 6.1*, Computers and Structures, Inc. Berkeley, California 94701 USA. September 1997.

Douglas, B. M. and W. H. Reid. *Dynamic testing and system identification of bridges*. Proc. ASCE . 108(10), 1982, pp. 2295-2312.

Halling, M.W., Achter, J.L., Womack, K.C., Ghasemi, H., "Condition Assessment of full-scale bridge bents: the forced-vibration technique," submitted for publication, 1999a.

Halling, M.W., Muhammad, I., Womack, K.C., "Bridge condition assessment using dynamic field testing," submitted for publication, 1999b.

Lieven, N. A. J. and D. J. Ewins. *Spatial Correlation Of Mode Shapes, The Coordinate Modal Assurance Criterion (COMAC)*. In Proceedings of the Sixth International Modal Analysis Conference, Kissimmee, Florida, February 1988, pp. 3042-3063.

Liu, Pei-Ling (1995). *Identification and damage detection of trusses using modal data.* J. Struct. Engrg., ASCE, 121(4), 599-608.

Liu, S. C., and Yao, J. T. P. (1978). *Structural identification concept.* J. Struct. Div., ASCE, 104(12), 1845-1858.

Muhammad, I., System Identification of Damage and Retrofit of Full-Scale Bridge Span, Ph.D. Dissertation, Utah State University, 1999.

Muhammad, I., Halling, M. W., Womack, K. C., "Forced vibration testing of a full-scale bridge span," proceedings, 1999, Transportation Research Board annual meeting, January, 1999.

Pandey, A. K., Biswas, M., and Samman, M. M. (1991). *Damage detection from changes in curvature mode shapes.* J. Sound. Vib., 145(2), 321-332.

Robinson, M., Condition Assessment of a Six Span Full-Scale Bridge Using Forced Vibration, Master's thesis, Utah State University, 2000.

Robinson, Marc J., Marvin W. Halling, Kevin C. Womack (2000) "Condition assessment of a six span full-scale bridge using forced vibration". Proc. SPIE 7'th Annual international symposium on smart structures and materials. Newport beach, California.

Salawu, O.S., and Williams, C., *Bridge Assessment Using Forced-Vibration Testing*, Journal of Structural Engineering, ASCE. Vol. 121, No. 2, pp. 161-173, 1995.

Tsai, W.H., and Yang, J.C.S. *Nondestructive Evaluation Of Composite Structures Using System Identification,* J. Engrg. Mat. And Tech., Vol. 110, No. 2, pp. 134-139, 1988.